Bio-optical properties of oceanic waters: A reappraisal

André Morel

Laboratoire de Physique et Chimie Marines, Université Pierre et Marie Curie, CNRS-INSU
Villefranche-sur-mer, France

Stéphane Maritorena

Institute for Computational Earth System Science, University of California, Santa Barbara, California

Abstract. The apparent optical properties (AOPs) of oceanic case 1 waters were previously analyzed [*Morel*, 1988] and statistically related to the chlorophyll concentration ([Chl]) used as a global index describing the trophic conditions of water bodies. From these empirical relationships a bio-optical model of the upper layer was developed. With objectives and structure similar to those of the previous study the present reappraisal utilizes AOPs determined during recent Joint Global Ocean Flux Study cruises, namely, spectral attenuation for downward irradiance $K_d(\lambda)$ and irradiance reflectance $R(\lambda)$. This revision also benefits from improved knowledge of inherent optical properties (IOPs), namely, pure water absorption coefficients and particle scattering and absorption coefficients, and from better pigment quantification (via a systematic use of high-performance liquid chromatography). Nonlinear trends, already observed between optical properties and algal biomass, are fully confirmed, yet with numerical differences. The previous $K_d(\lambda)$ model, and subsequently the $R(\lambda)$ model, is modified to account for these new relationships. The $R(\lambda)$ values predicted as a function of [Chl] and the predicted ratios of reflectances at two wavelengths, which are commonly used in ocean color algorithms, compare well with field values (not used when developing the reflectance model). This good agreement means that semianalytical ocean color algorithms can be successfully applied to satellite data. Going further into purely analytical approaches, ideally based on radiative transfer computations combined with a suite of relationships between the IOPs and [Chl], remains presently problematic, especially because of the insufficient knowledge of the phase function and backscattering efficiency of oceanic particles.

1. Introduction

Some 12 years ago, and almost simultaneously, two papers were published [*Gordon et al.*, 1988; *Morel*, 1988] with the purpose of reviewing the cumulated knowledge about the optical properties of oceanic waters and analyzing the data acquired in the 1970s and early 1980s. Case 1 waters [*Morel and Prieur*, 1977], namely, the waters for which algal cells (phytoplankton) and their associated living or inanimate materials (heterotrophic organisms, including bacteria; various debris; and excreted organic matter) are the optically significant components, were particularly studied. To the extent that the global quantification of these biogenous materials is operationally and routinely made through the determination of a major pigment, namely, chlorophyll a, the optical properties of case 1 waters depend (by definition) on, and have naturally been related to, their chlorophyll concentration, denoted [Chl]. On the basis of such empirical relationships, models were developed allowing apparent optical properties (AOPs) [*Preisendorfer*, 1961], such as the spectral diffuse attenuation coefficients for downward irradiance $K_d(\lambda)$ and the irradiance reflectance spectrum $R(\lambda)$, to be predicted from the chlorophyll concentration (see review given by *Mobley* [1994]).

A revision of the previous findings is timely for several rea-

sons. New and improved field data, generally collected during Joint Global Ocean Flux Study (JGOFS) cruises, are now available. For example, the database for $K_d(\lambda)$ or $R(\lambda)$ has increased considerably and pigment determinations are more accurate thanks to the introduction and systematic use of high-performance liquid chromatography (HPLC) techniques capable of discriminating a large suite of pigments (chlorophylls, pheopigments, and carotenoids). The inherent optical properties (IOPs) are also better documented than 10 years ago. The beam attenuation coefficient at 660 nm, along with the algal chlorophyll fluorescence, has been routinely measured at sea, providing new insights into the relationship between the chlorophyll content and the scattering coefficient of the particle population [*Loisel and Morel*, 1998]. The variations of light absorption coefficient of marine particles in oceanic waters were recently analyzed as a function of the chlorophyll concentration [e.g., *Garver et al.*, 1994; *Bricaud et al.*, 1998]. Finally, and perhaps more importantly, recent measurements of the absorption spectrum of pure water [*Sogandares and Fry*, 1997; *Pope and Fry*, 1997] have important implications on both the interpretation of field data and ocean color modeling.

The main goal of the present paper is to analyze these new data, the $K_d(\lambda)$ data in particular, in the same way as was previously done [*Morel*, 1988] (hereinafter referred to as JGR88), and, subsequently, to propose modified parameterizations by which K_d can be related to (and predicted from)

Table 1. Relevant Information Concerning the Cruises and the Optical Data Used in the Present Study and Forming the New Data Subset

Year	Cruise	Vessel	Zone	(Chl) Range[a]	$K_d(\lambda)$	$R(\lambda)$
1986	PACIPROD	*Charcot*	Peru-Galapagos	0.21–5.45	—[b]	41
1987	CHLOMAX	*Suroit*	Sargasso Sea	0.040–0.067	—[c]	13
1991–1992	EUMELI 3–4	*Atalante*	NE tropical Atlantic	0.042–2.40	36	32
1994	OLIPAC	*Atalante*	central tropical Pacific	0.043–0.295	61	109
1996	MINOS	*Suroit*	Mediterranean Sea	0.035–0.089	24	10
Total					121	205[d]

[a]Determined via spectrophotometry (PACIPROD), spectrofluorometry (CHLOMAX), and HPLC (other cruises).

[b]The 21 K_d spectra from the Paciprod cruise were already included in the database used in 1988; the 41 $R(\lambda)$ reflectance spectra were not considered by *Gordon and Morel* [1983, Figure 3b] nor by the 1988 database.

[c]Only the reflectance spectra are available for this cruise.

[d]Some other reflectance values, determined at discrete wavelengths with a SPMR radiometer (Satlantic Inc.) during the Almofront-2 cruise (Alboran Sea, January 1998; F. Fell, unpublished data, 1999), are also used in Figures 11a and 11b.

[Chl]. From these empirical relationships a modified reflectance model will be derived and tested against new $R(\lambda)$ data.

Case 1 waters, in essence, constitute a two-component system, with water on the one hand and the "biological compartment" on the other hand. The latter is complex as it includes all particulate and dissolved materials, living and inanimate, created through the biological activity initiated by algal photosynthesis. Moreover, neither the proportion between the chlorophyll content and the algal biomass nor that between the algal biomass and the rest of the derived biogenic matter is constant. Therefore, if general trends emerge, and actually have been captured in the past, the noisy nature of relationships between the single quantity [Chl] and any of the bulk optical properties determined by the whole biogenic compartment is in no way surprising. For a long time [e.g., *Gordon and Morel*, 1983] it has been acknowledged that the skill of models based on such empirical relationships has to be evaluated in a statistical sense. Case-by-case deviations inevitably occur between observed properties and the average values predicted from the sole chlorophyll concentration. Even systematic deviations have been repeatedly recorded in specific zones, as in the Southern Ocean [*Mitchell and Holm-Hansen*, 1991]. In previous studies the exact amplitude of the natural variability was difficult to assess mostly because some of the scatter in the data was likely to result from experimental deficiencies and changing methodologies (in the pigment determination, for instance). With improved methodologies this artifact hopefully reduces, so a reevaluation of this variability becomes, in principle, feasible.

A complementary purpose of the present work is to explore the capacity of interpreting the empirical relationships between [Chl] and AOPs through an analytical way based on direct relationships between IOPs and [Chl], as recently determined. Not all IOPs are presently known with a sufficient accuracy (the backscattering coefficient, for instance); therefore, as a corollary, the gaps that still hamper progress in the development of bio-optical models must be identified.

2. Data and Methods

The optical and pigment data obtained during several recent cruises, all in case 1 waters, are summarized in Table 1. They constitute what is hereinafter referred to as the "new data subset," whereas the previous data (JGR88, Table 1) will be denoted as the "old data subset." It is worth remarking that except for a few determinations the new subset is largely dominated by measurements conducted in oligotrophic waters, with chlorophyll concentrations below 0.3 mg m^{-3}. Nevertheless, during the cruise Eutrophy, Mesotrophy, and Oligotrophy (EUMELI) 4 in the tropical Atlantic some mesotrophic as well as eutrophic waters were studied (with [Chl] between 1 and 4 mg m^{-3}, approximately). In general, however, low to extremely low chlorophyll values were systematically observed, namely, in the tropical Pacific (Oligotrophy in Pacific (OLIPAC) cruise), in the oligotrophic site of the EUMELI program, and in the Mediterranean Investigation of Oligotrophic Systems (MINOS) cruise. Therefore the new data subset complements the old one. Indeed, the old subset included 176 case 1 waters (see JGR88, Figure 5a) and spanned a wider chlorophyll range (0.02–>30 mg m^{-3}), but data from oligotrophic regimes were scarce, as no more than 10 data dealt with concentrations below 0.1 mg m^{-3}.

For all recent cruises in Table 1 the pigment determinations were always made using HPLC with separate assessments of monovinyl and divinyl chlorophyll a [*Claustre*, 1994]. Hereinafter the quantity [Chl] is defined as the sum of the concentrations in these two photosynthetic pigments when they are both present (always in oligotrophic waters here studied). When using the HPLC technique, pheopigments in the upper layers of the open ocean were generally found insignificant compared to active chlorophyll a. Consequently, the notation used here, [Chl], differs from that employed by JGR88, where the symbol "C" (commonly adopted at that time) was the sum of active chlorophyll a and its degraded derivative form pheophytin a, which was often (and erroneously) found in notable proportions. It is now acknowledged that a methodological ambiguity inherent to fluorimetric technique has historically led to an overestimate of the pheopigment content when chlorophyll b is present [*Gibbs*, 1979]. This is no longer the case with HPLC, so the chlorophyll and the pheopigment concentrations are well defined. Very small (<10%) amounts of pheophytin were sometimes detected; in such cases this concentration was simply included within the quantity denoted [Chl]. A fluorometer (FL 3000, SeaTech Inc.) was systematically operated in conjunction with a conductivity-temperature-depth (CTD) sensor. The vertical profiles of algal fluorescence were converted into equivalent [Chl] profiles by using the HPLC values obtained on discrete samples (examples in Figure 1). Mean [Chl] values were computed by integrating these vertical
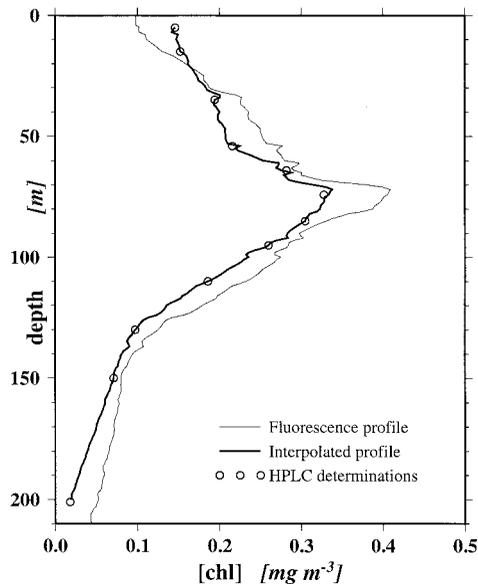
Figure 1. Example of the transformation of the in situ fluorescence profile into chlorophyll *a* (monovinyl and divinyl) profile based on HPLC discrete determinations made at 12 levels (OLIPAC, 150°W, 5°S, November 19, 1994).

continuous profiles from beneath the surface down to a certain depth Z corresponding to optical measurement (see below). This method has been preferred to the trapezoidal integration based on the discrete measurements.

During the EUMELI 3 and 4 cruises the spectral values of downward irradiance $E_d(\lambda)$ were measured at discrete depths with a custom-built instrument, also used during the previous campaigns (which led to the old data subset). Over time the data acquisition module of this instrument has been improved, but its optical arrangement remained basically unchanged. For the OLIPAC and MINOS cruises a calibrated LICOR® instrument (LI-1800 UW) was operated. Whatever the instrument, the $E_{d,Z}(\lambda)$ spectra were obtained in rapid succession at different depths Z and were corrected for the slight shift in incoming solar radiation (monitored on the deck) during the course of the experiment. Note that all measurements here considered were performed near the solar noon in sunny and steady conditions. Ship shadow influence is avoided thanks to a long crane operated from the stern and oriented in the direction of the Sun; the ship orientation is maintained in such a way that the Sun remains off the stern during the optical cast. The spectra corresponding to the same incident radiation are thus compatible for a straightforward calculation of the diffuse attenuation coefficients for downward irradiance $K_d(\lambda)$; this spectral coefficient is computed for a layer extending from the surface down to a certain depth Z according to

$$K_d(\lambda) = Z^{-1} \ln [E_{d,0-}(\lambda)/E_{d,Z}(\lambda)]. \quad (1)$$

$E_{d,0-}(\lambda)$, which represents the downwelling irradiance just beneath the air-water interface $(0-)$, is derived from the measurement performed above the water by applying a transmittance factor 0.965 regardless of the wavelength. This corrective factor accounts for the loss by reflection at the interface and is valid [see *Morel and Antoine*, 1994, Figure A1] for zenith solar angles $\theta_0 < 45°$ and for conditions as encountered during these cruises (clear skies, low wind, and experiments made around

noon with small θ_0 values). The choice of the depth Z is examined below.

In highly transparent blue waters, typical of the new data set, the light field fluctuations caused by surface waves are important within the upper layer, so that downward irradiance spectra are characteristically noisy at shallow depths. More generally, in such waters, noise-free downward irradiance spectra were recorded with the custom-built radiometer (scanning speed ~4 s for a 400–700 nm spectrum) once the instrument reached 15 or 20 m and were recorded with the LICOR sensor (scanning speed ~25 s for a 310–750 nm spectrum) once the instrument reached about 25–30 m. This experimental limitation has an important consequence. In effect, the red part of the $E_d(\lambda)$ spectrum (for $\lambda > 590–600$ nm) either cannot be obtained (with the old sensor), or if determined (as it is in the case with the LICOR instrument), it cannot be exploited for reasons exposed below.

With the old instrument the automatically adjusted gain allows radiometric measurements (at each depth) to be obtained over 2 decades, so that any (red) signal vanishes within the noise when it becomes <1% of the maximum signal. If this maximum is recorded in the blue or blue-green domain, which is the typical situation for low or moderate chlorophyll concentration, the signal in the red becomes undetectable at about 20 m. The irradiance within red part of the spectrum is distinctly above the noise and thus measurable only in extremely green waters with high chlorophyll content, when the E_d maximum shifts toward 565 nm (and when the high water absorption and scattering reduce the wave-focusing effect and thus allow shallower measurements to be successful). This instrumental drawback has already been discussed and led to a reduction of the available data for statistical analyses within the long-wavelength domain (see JGR88, Figure 6).

With the LICOR instrument the dynamical range is fixed. As it extends over more than 5 decades, there is no particular problem in measuring the weak red radiation, even at considerable depth. The limitation, no longer of radiometric origin, is here of physical nature. In the long-wavelength domain, the downward radiation, quickly absorbed, is progressively replaced by the inelastically scattered radiation, namely, the Raman emission and within a narrower band the chlorophyll fluorescence emission around 685 nm. To the extent that the first noiseless downward irradiance spectrum is generally determined at a depth as large as 30 m, the inelastic processes already interfere. Instances of the impact of these emissions, which increase with increasing depth by progressively depressing the $K_d(\lambda)$ spectrum at large (>600 nm) wavelengths, are displayed in Figure 2. Even at the shallowest depth, the deformation of the spectrum occurs, as simply demonstrated by the fact that K_d is smaller than the absorption coefficient for pure water in the red part of the spectrum. Correcting for such effects, and restoring the K_d values, as they would be in absence of transspectral phenomena, is theoretically feasible. However, uncertainties still remain in such a procedure, and it is presently safer to discard the K_d values in this spectral domain.

Because the upper layer (limited to the first "penetration depth") [*Gordon and McCluney*, 1975] is of interest for remote sensing application, the rule was adopted to consider only one depth interval, between the surface and the depth of the first good (i.e., noise-free) $E_d(\lambda)$ spectrum. Actually, this depth slightly exceeds that of penetration (defined as $1/K_d$), except in the blue part of the spectrum. Computations according to
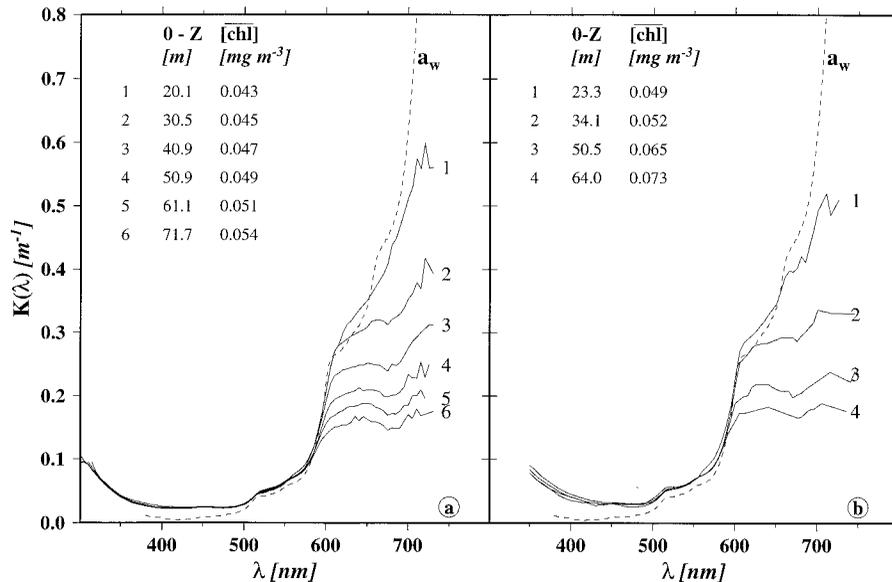
Figure 2. Spectra of the diffuse attenuation coefficient for downward irradiance computed between surface, 0^-, and various depths Z as indicated: (a) Pacific Ocean (150°W, 16°S, November 27, 1994) and (b) Mediterranean Sea (17°E, 37°N, 1996). Note that the [Chl] concentrations at these two stations are similar, and that successful measurements at about 20 m, as shown here, were exceptional when using the LICOR instrument. The mean Chl concentrations for the layers considered (obtained by integrating Chl profiles such as that one shown in Figure 2) are also given. The absorption spectrum (labeled a_w) for pure water [*Pope and Fry*, 1997] is also displayed for comparison.

(1) obviously could be made for any other depth interval. Considering two layers, from 0 to Z_1 and then from 0 to Z_2 (or even the Z_1–Z_2 layer), practically provides redundant information, to the extent that within the upper mixed layer the chlorophyll concentration and optical properties are not changing much. Therefore only one attenuation spectrum is selected per experiment. However, several experiments often were performed at a same location but at different times and with independent pigment determinations; they are included in the present analysis.

The irradiance reflectance, or irradiance ratio R, is defined as the ratio of upward (E_u) to downward (E_d) irradiances; its spectral value is

$$R(\lambda) = E_u(0-, \lambda)/E_d(0-, \lambda), \qquad (2)$$

where both spectral irradiances are ideally determined at "null" depth (0−). The downwelling irradiance spectrum, actually measured above the water, is corrected as said before (by using the 0.965 factor). $E_u(\lambda)$ is measured far from the ship (10–15 m) at a depth as small as possible (about 1–2 m), compatible with the sea state and ship motions. Both irradiances are normalized to a constant incident solar flux. When determinations of $E_u(\lambda)$ were not possible close to the surface because of the sea state, an extrapolation from several spectra determined at greater depths was attempted to infer E_u at null depth. This procedure, however, requires that the instrument be steady enough and that its depth be accurately known (which is not the case in general), so most of these data were simply discarded.

As for K_d, there may be several independent determinations of R at the same geographical location. Note that these two quantities (R and K_d) are obtained by forming ratios of irradiances measured by a unique sensor. They are therefore independent from the spectral calibration of the instrument. The

immersion factor and its spectral dependency, however, are involved in the derivation of $R(\lambda)$.

3. Analysis, Results, and Modeling

Statistical regression analysis of the reflectance data against the chlorophyll concentration represents the so-called empirical way to derive algorithms for the ocean color interpretation [see, e.g., *O'Reilly et al.*, 1998; *Gordon and Morel*, 1983, Table 2]. This approach will not be employed here. Rather, the $R(\lambda)$ data set will serve as a test bench for a semianalytical reflectance model. Some empiricism, indeed, remains incrusted as the reflectance model is developed from the statistical analysis of the $K_d(\lambda)$ in relation to [Chl] combined with other results related to the scattering coefficient [*Loisel and Morel*, 1998].

3.1. Empirical Relationships Between Spectral Values of the Diffuse Attenuation Coefficient and the Chlorophyll Concentration

In what follows, K_d, the attenuation coefficient for downward irradiance, will be simply denoted K. The analysis is made here in the same way as previously (JGR88) and consists of studying the quantities $[K(\lambda) - K_w(\lambda)]$ along with [Chl]; this approach assumes that by approximation, $K(\lambda)$ can be considered as the sum of $K_w(\lambda)$, a term for pure water, and K_{bio}, a term merging the contributions of all biogenic components, namely, algal cells, associated nonalgal organisms (such as viruses, heterotrophic bacteria, and other small heterotrophs), various detritus, dissolved organic colored matter, and perhaps bubbles [*Stramski*, 1994; *Zhang et al.*, 1998], so that

$$K(\lambda) = K_w(\lambda) + K_{bio}(\lambda). \qquad (3)$$

Then K_{bio} at each wavelength is related to Chl by performing a linear regression analysis on the log-transformed quantities
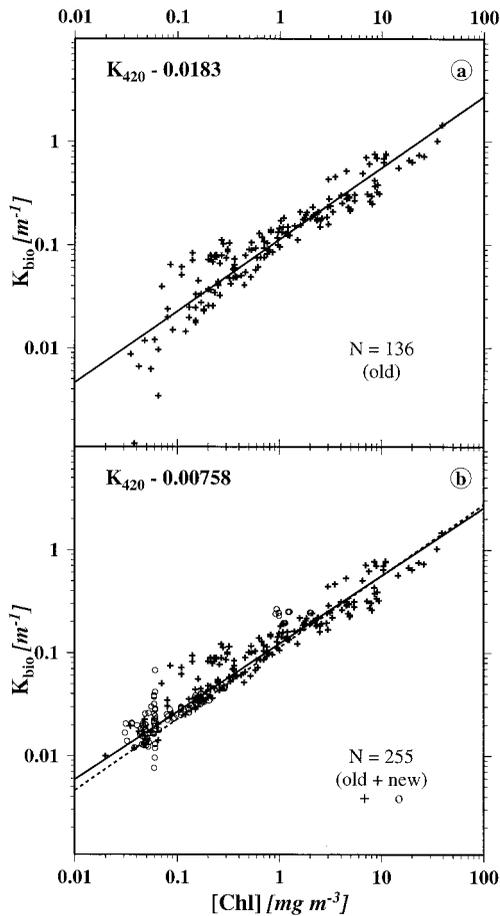
Figure 3. Log-log plot of $K_{bio}(420)$ as a function of the Chl concentration for the wavelength 420 nm: (a) the old data set and previous regression line (JGR88) and (b) all data pooled together; the new regression line is displayed as a solid straight line, while the old one, redrawn from Figure 3a, is shown as the dashed line.

$y = \log (K - K_w)$ and $x = \log$ [Chl]. The coefficient K_w, to be subtracted from K, is by approximation expressed as

$$K_w(\lambda) = a_w(\lambda) + (1/2)b_w(\lambda), \qquad (4)$$

where a_w and b_w stand for the absorption and scattering coefficients of optically pure sea water, respectively. This expression actually underestimates K_w, and a more accurate formulation could be adopted [*Gordon*, 1989]. However, this is not an important issue here because once the statistical relationships between K_{bio} and [Chl] are established, the predicted K (as a function of [Chl]) is obtained by re-adding (according to (3)) the K_w value that was initially subtracted. Therefore the final result does not depend heavily on the adopted K_w value (at least if not dramatically wrong). A misestimate of K_w essentially would result (and actually does, as shown later) in deteriorating the goodness of the fit in the statistical relationship; this is particularly true when K becomes close to K_w (i.e., at very low chlorophyll concentration). This is illustrated in the comparison of the previous and present results.

Figure 3a, restricted to the old data set, is strictly identical to Figure 7a by JGR88, except that 420 nm is used instead of 450 nm; the K_w coefficient (0.0183 m^{-1}), which was derived from the a_w values of *Smith and Baker* [1981], is kept unchanged. In

Figure 3b the K_w value (0.00758 m^{-1}) is based on the recent absorption values of pure water of *Pope and Fry* [1997]. Note that the wavelength 420 nm has been purposely selected for this comparison since the change in the a_w values is maximal at this wavelength (0.00454 m^{-1} [*Pope and Fry*, 1997] versus 0.0153 m^{-1} [*Smith and Baker*, 1981]). Because a smaller K_w value is subtracted from K, the points (for [Chl] <0.2 mg m^{-3}) that were lying well below the regression line in Figure 3a are now closer to it (Figure 3b). Therefore, with a reduced scatter and no biased trend in this domain the overall fit is improved ($r^2 = 0.96$ instead of 0.92). The new subset is also plotted on Figure 3b and confirms the improved alignment of the points. Interestingly, the general trend, previously observed over the entire chlorophyll range (which was spanning about 3 orders of magnitude), is not altered by the inclusion of the new data. Accordingly, when all (old + new) data are pooled together and when Pope and Fry's spectral absorption values are systematically used, the new regression lines differ from the previous ones, yet the changes are not drastic. From these linear regression analyses made on the log-transformed data (wavelength increment 5 nm), $K_{bio}(\lambda)$ coefficients can be expressed as power laws:

$$K_{bio}(\lambda) = \chi(\lambda)(Chl)^{e(\lambda)}. \qquad (5)$$

With more data and less dispersion at low [Chl] concentrations the correlation coefficients are notably higher than those previously obtained with the old data set (combined with
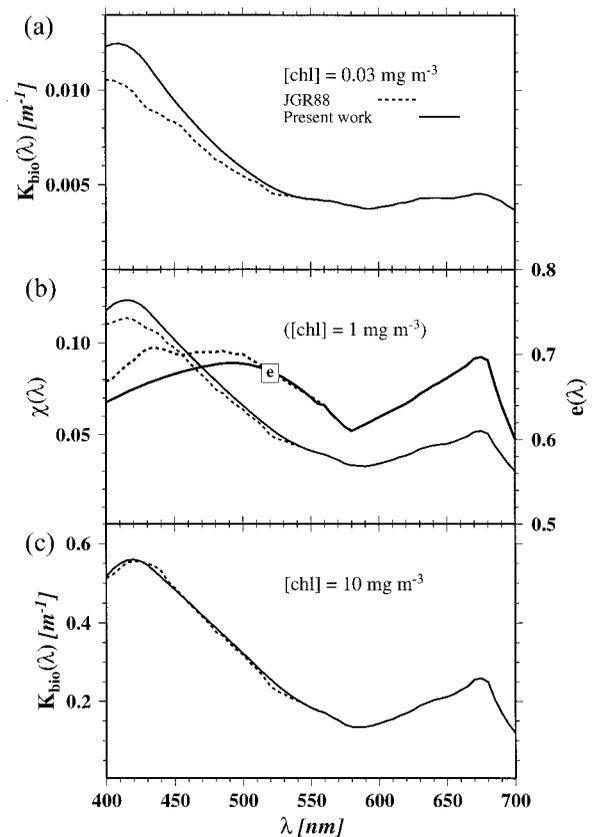

Figure 4. Spectral values of K_{bio} for three chlorophyll concentrations, as indicated. When [Chl] = 1 mg m^{-3}, $K_{bio}(\lambda) = \chi(\lambda)$; the exponent $e(\lambda)$ is also displayed (Figure 4b). The solid lines and dashed lines are for the new and old regression analyses, respectively.
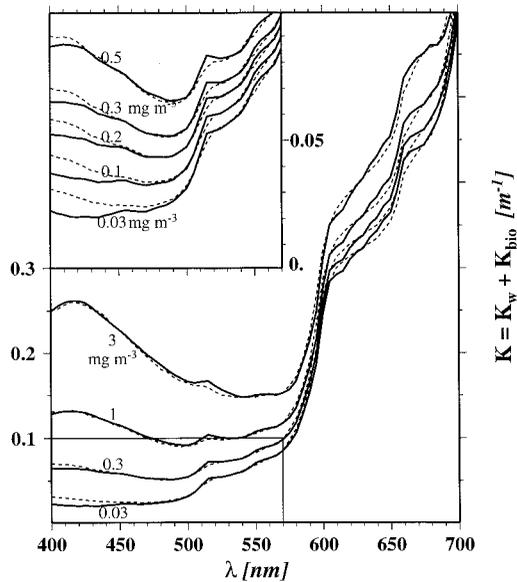
Figure 5. Spectral values of $K = K_w + K_{bio}$ for various chlorophyll concentrations, as indicated. An enlargement of the blue part of the spectrum for low chlorophyll contents is provided in the inset. The solid and dashed lines are for the new and old regression analyses, respectively.

higher K_w values). The changes in the K_{bio} spectrum with various chlorophyll concentrations are displayed in Figure 4, and those changes in $K(\lambda)$ (equation (3)) are displayed in Figure 5. The previous (JGR88) results are redrawn in Figures 4 and 5 for the sake of comparison. Examples of the differences between actual K_{bio} values and the ones derived from (5), used as a model, will be shown and discussed later (Figure 14).

The updated $\chi(\lambda)$ coefficients and $e(\lambda)$ exponents are given in Table 2 (to be compared to Table 2 of JGR88). The maximal deviations occur in the blue part of the spectrum (400–500 nm), essentially because of the use of pure water absorption data from *Pope and Fry* [1997], which are considerably lower than was previously believed. In the 500–590 nm domain the differences tend to lessen as the new values of χ and e are practically identical to the previous ones (see Figure 4b). Because the new data set cannot be exploited for wavelengths larger than 590–600 nm, the previous values are not revised.

These modified χ and e values (Figure 4b) do not result in modifying $K_{bio}(\lambda)$ when (Chl) is high (Figure 4c); in contrast, the K_{bio} values for oligotrophic waters (Figure 4a) are distinctly higher in the blue part of the spectrum than the previous values. The spectral shape is also clearly modified. Indeed, a maximum centered on 420 nm still persists at low (Chl), while a featureless ascending slope resulted from the previous anal-

Table 2. Spectral Values Resulting From the Present Statistical Analysis for the Three Parameters Appearing in (3), (4), and (5)

λ, nm	K_w, m^{-1}	e	χ	λ, nm	K_w, m^{-1}	e	χ
350	0.02710	0.77800	0.15300	530	0.04454	0.67224	0.04829
355	0.02380	0.76700	0.14900	535	0.04630	0.66739	0.04611
360	0.02160	0.75600	0.14400	540	0.04846	0.66195	0.04419
365	0.01880	0.73700	0.14000	545	0.05212	0.65591	0.04253
370	0.01770	0.72000	0.13600	550	0.05746	0.64927	0.04111
375	0.01595	0.70000	0.13100	555	0.06053	0.64204	0.03996
380	0.01510	0.68500	0.12700	560	0.06280	0.64000	0.03900
385	0.01376	0.67300	0.12300	565	0.06507	0.63000	0.03750
390	0.01271	0.67000	0.11900	570	0.07034	0.62300	0.03600
395	0.01208	0.66000	0.11800	575	0.07801	0.61500	0.03400
400	0.01042	0.64358	0.11748	580	0.09038	0.61000	0.03300
405	0.00890	0.64776	0.12066	585	0.11076	0.61400	0.03280
410	0.00812	0.65175	0.12259	590	0.13584	0.61800	0.03250
415	0.00765	0.65555	0.12326	595	0.16792	0.62200	0.03300
420	0.00758	0.65917	0.12269	600	0.22310	0.62600	0.03400
425	0.00768	0.66259	0.12086	605	0.25838	0.63000	0.03500
430	0.00770	0.66583	0.11779	610	0.26506	0.63400	0.03600
435	0.00792	0.66889	0.11372	615	0.26843	0.63800	0.03750
440	0.00885	0.67175	0.10963	620	0.27612	0.64200	0.03850
445	0.00990	0.67443	0.10560	625	0.28400	0.64700	0.04000
450	0.01148	0.67692	0.10165	630	0.29218	0.65300	0.04200
455	0.01182	0.67923	0.09776	635	0.30176	0.65800	0.04300
460	0.01188	0.68134	0.09393	640	0.31134	0.66300	0.04400
465	0.01211	0.68327	0.09018	645	0.32553	0.66700	0.04450
470	0.01251	0.68501	0.08649	650	0.34052	0.67200	0.04500
475	0.01320	0.68657	0.08287	655	0.37150	0.67700	0.04600
480	0.01444	0.68794	0.07932	660	0.41048	0.68200	0.04750
485	0.01526	0.68903	0.07584	665	0.42947	0.68700	0.04900
490	0.01660	0.68955	0.07242	670	0.43946	0.69500	0.05150
495	0.01885	0.68947	0.06907	675	0.44844	0.69700	0.05200
500	0.02188	0.68880	0.06579	680	0.46543	0.69300	0.05050
505	0.02701	0.68753	0.06257	685	0.48642	0.66500	0.04400
510	0.03385	0.68567	0.05943	690	0.51640	0.64000	0.03900
515	0.04090	0.68320	0.05635	695	0.55939	0.62000	0.03400
520	0.04214	0.68015	0.05341	700	0.62438	0.60000	0.03000
525	0.04287	0.67649	0.05072				

ysis; this slope was interpreted as a predominant effect of nonalgal, blue absorbing, detritic materials (this point will be examined later, when discussing the K values in the UV domain).

The new $K_w(\lambda)$ values (also listed in Table 2) differ from the previous ones not only in the blue part of the spectrum but also in the vicinity of specific shoulders (at 515, 605, and 662 nm) related to high-order resonance modes of the water molecule [*Tam and Patel*, 1979; *Sogandares and Fry*, 1997]. When added to K_{bio}, they produce $K(\lambda)$ spectra (Figure 5), which differ notably from the previous ones in oligotrophic waters ([Chl] below 0.3 mg m^{-3}) especially within the spectral range below 500 nm. Interestingly, the minute maximum that occurs at 450 nm in the $K(\lambda)$ spectra at low chlorophyll concentration (and actually originates from water absorption related to the seventh harmonic of the O-H stretch) is confirmed by field experiments (Figure 2). The maximum in K_{bio}, which occurs at 420 nm, is compensated by the minimum in K_w, so that the $K(\lambda)$ spectrum is rather flat in this spectral domain. This prediction (Figure 5 inset) is fully confirmed by detailed observation, as displayed in Figure 2.

3.2. Euphotic Depth and Chlorophyll Concentration

JGR88 used the $K(\lambda)$ analysis to relate the thickness of the euphotic layer (Z_e) to the mean pigment concentration within this layer (JGR88, Table 3) or to the column-integrated chlorophyll content (between 0 and Z_e). With the revised parameterization of $K(\lambda)$ the same computation produces Z_e values that do not appreciably differ from the previous ones for high or moderate [Chl] values. At low concentration (<0.3 mg m^{-3}), however, Z_e is slightly increased (Figure 6) when the new, lower $K(\lambda)$ values are used. The curvature in the domain of low [Chl] accounts for the fact that Z_e tends toward a limiting value determined by pure water absorption. Actually, euphotic depths as large as 124–130 m were repeatedly observed during several days in the Pacific Ocean (150°W, 16°S; same location as for Figure 10a); such values agree with these revised Z_e values when predicted for the mean [Chl] value (around 0.075 mg m^{-3}) computed between 0 and Z_e at this station. The previous relationship would have led to an (underestimated) 115 m euphotic depth.

In view of predicting the euphotic depth from a vertical chlorophyll profile it is convenient to integrate progressively the column content to obtain simultaneously [Chl$_{tot}$] and Z_e through an iterative process (described by *Morel and Berthon* [1989]). The quantity [Chl$_{tot}$] is also plotted as a function of Z_e in Figure 6. For computational convenience this curve can be approximated by two successive linear segments (in the log-log domain), leading to the following expressions:

$$Z_e = 912.5 \, [\text{Chl}_{tot}]^{-0.839} \qquad 10 \text{ m} < Z_e < 102 \text{ m},$$
$$Z_e = 426.3 \, [\text{Chl}_{tot}]^{-0.547} \qquad 102 \text{ m} < Z_e < 180 \text{ m}. \tag{6}$$

The common point for $Z_e = 102$ m corresponds to [Chl$_{tot}$] = 13.65 mg m^{-2} instead of (exactly) to 10.00 mg m^{-2} in the previously proposed expressions [*Morel and Berthon*, 1989]. Polynomials expressions relating the decimal logarithms of Z_e and of [Chl$_{tot}$] can also be used (see Figure 6).

3.3. Possible Extension of the $K(\lambda)$ Coefficients Toward the Near-UV Domain

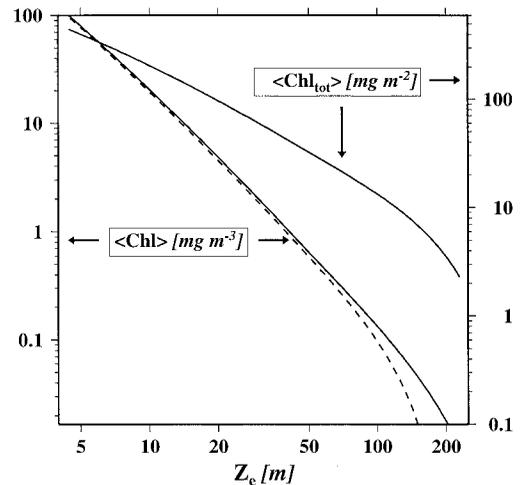There are few measurements of the K coefficient in this spectral domain. To our knowledge the only available data

Figure 6. Euphotic depth Z_e as a function of the mean chlorophyll concentration within this layer (left-hand ordinate scale) according to the previous (JGR88) $K(\lambda)$ parameterization (dashed curve) and computed through the present parameterization (solid curve). Column-integrated chlorophyll content, [Chl$_{tot}$], is also plotted as a function of Z_e (right-hand scale); by approximation this curve can be replaced by two linear portions (see (6)) or by a polynomial of order 4 relating $\log_{10}(Z_e)$ and $\log_{10}$ [Chl$_{tot}$] with the constant $a_0 = 2.1236$ and the following a_1 to a_4 coefficients 0.932468, -1.4264, 0.52776, and -0.07617, respectively; this expression is appropriate for Z_e between the depths 5 and 180 m.

related to varying chlorophyll concentration are those of *Smith and Baker* [1981] and *Baker and Smith* [1982]. They have been tentatively used by *Morel and Antoine* [1994] to extrapolate $\chi(\lambda)$ and $e(\lambda)$ below 400 nm. The present data include $K(\lambda)$ determinations extended down to 305 nm (OLIPAC cruise) or to 350 nm (MINOS cruise), all related to low (Chl) waters.

A systematic analysis of these data, however, is not feasible, all the more because the K_w values still remain uncertain in the UVA and UVB domains. The revised absorption values for pure water begin at 380 nm by *Pope and Fry* [1997] and at 340 nm by *Sogandares and Fry* [1997]; the corresponding K_w values for these wavelengths would be 0.0167 and 0.0402 m^{-1}, respectively. Other absorption values can be found in the previous literature showing considerable divergences (see below). Although a complete discussion is not yet possible, the examination of the new data set leads to several remarks.

1. The K values near 305 nm (about 0.095 m^{-1}; Figure 2), as observed in oligotrophic waters of the tropical Pacific, are appreciably below those proposed by *Smith and Baker* [1981] for pure water ($K_w = 0.154$ m^{-1}) and those used by *Morel and Antoine* [1994]. Such low, or even lower, K_d values were also observed in Antarctic ice-covered lakes [*Vincent et al.*, 1998], where the amount of chromophoric dissolved organic matter (CDOM) is reduced because catchment vegetation is almost nonexistent in such environments. These very low field values would be compatible with the absorption values for pure water published by *Boivin et al.* [1986], namely, 0.041 m^{-1} at 313 nm, or by *Quickenden and Irvin* [1980], 0.03 m^{-1} at 300 nm. There is an obvious need for accurate determinations of absorption by pure water in this spectral domain.

2. The OLIPAC and MINOS data have been tentatively analyzed in the near-UV domain (Figure 7) in a way similar to that used for the visible part (Figure 3) and using the revised
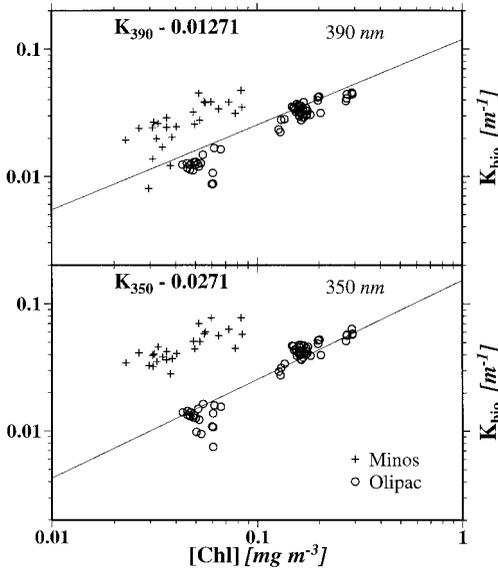
Figure 7. As in Figure 3b, but for 390 and 350 nm. The lines corresponding to 0.119 [Chl]$^{0.67}$ and 0.153 [Chl]$^{0.778}$, for $\lambda =$ 390 and 350 nm, respectively, are drawn using the values proposed by *Morel and Antoine* [1994].

K_w values. The two data sets, in spite of similar chlorophyll content, systematically diverge with respect to their K_{bio} coefficients. The difference, which regularly increases with decreasing wavelength (Figure 7), suggests that the effect of CDOM, or of colored (nonalgal) particles, is more marked in the semienclosed Mediterranean Sea than in open Pacific waters. Actually, even in the visible part of the spectrum, at 440 nm the nonalgal particle contribution to total particle absorption is distinctly higher (about 70% on average) in the Mediterranean than in the Pacific, where it is at its minimum, namely, below 15% [see *Bricaud et al.*, 1998, Figure 2].

3. The spectral values for χ and e, previously proposed in the near-UV domain [*Morel and Antoine*, 1994], seem to be adequate in reproducing the data from the Pacific and perhaps are representative of a kind of lower limit for diffuse attenuation in oligotrophic waters. As such, they are repeated in Table 2 (limited to 350 nm, however). These χ and e values, however, are not appropriate for the Mediterranean Sea data. Such location-dependent and systematic deviations demonstrate that when scrutinized, case 1 waters do not always behave in strictly identical ways. The reflectance spectra, examined later (Figure 10c), confirm the existence of differing behaviors and of "nuances" inside case 1 waters, according to the location.

3.4. Modeling Reflectance Spectra

The empirical relationships established between $K(\lambda)$ and [Chl] can be used to build a reflectance model by which the spectral values of reflectance $R(\lambda)$, at null depth, can be predicted from the chlorophyll concentration in the upper layer. Radiative transfer studies [*Gordon et al.*, 1975; *Prieur*, 1976; *Morel and Prieur*, 1977] have shown that by approximation, R can be simply expressed as a function of the ratio of the backscattering coefficient b_b to the absorption coefficient a according to

$$R(\lambda) = f[b_b(\lambda)/a(\lambda)] \qquad (7)$$

provided that b_b remains small compared to a (as is usually found in case 1 waters); if not, the denominator must include the sum of a and b_b. The f factor above varies [*Kirk*, 1984; *Gordon*, 1989] with the illumination conditions at the surface (essentially with the Sun position for clear skies). Given an incident radiant field, f also depends on the inherent optical properties of the water body and thus on the chlorophyll concentration and wavelength [*Morel and Gentili*, 1991]. In what follows, the procedure developed by JGR88 to generate $R(\lambda)$ will be used with some modifications to account for some recent findings. Below is a brief reminder of this iterative scheme.

In essence, this scheme consists of introducing $b_b(\lambda)$ (its value is discussed later) in (7) and replacing $a(\lambda)$ by $u_1 K(\lambda)$, where $u_1 = 0.75$, whatever the wavelength (and f is set to the oft used value 0.33). A first set of $R(\lambda)$ values is thus derived. Then an exact relationship (derived from the Gershun's equation), namely,

$$a = K_d \mu_d [1 + R(\mu_d/\mu_u)]^{-1}[1 - R + (K_d)^{-1} dR/dZ], \qquad (8)$$

is operated with some simplifications, namely, by letting μ_u equal 0.40, letting μ_d equal 0.90, and neglecting dR/dZ, which results in

$$a(\lambda) = K_d(\lambda)0.90[1 + 2.25R(\lambda)]^{-1}[1 - R(\lambda)] \qquad (8')$$

or

$$a(\lambda) = K_d(\lambda)u_2(\lambda). \qquad (8'')$$

The first set of $R(\lambda)$ values is used to produce the spectrally varying $u_2(\lambda)$ values through (8') and a new set of $a(\lambda)$ values through (8''). With these adjusted $a(\lambda)$ values, through a second loop using (7), a more accurate set of $R(\lambda)$ values is derived, and so forth. Stable $R(\lambda)$ values are obtained within three loops in this iterative process.

The derivation of the backscattering coefficient $b_b(\lambda)$ starts with the use of a mean empirical expression [*Gordon and Morel*, 1983], which relates the particle scattering coefficient b_p at 550 nm to [Chl], namely,

$$b_{p550}([\mathrm{Chl}]) = 0.30[\mathrm{Chl}]^{0.62}. \qquad (9)$$

Actually, this relationship was established for the total scattering coefficient b_{550} so that $b_{w\,550}$, the molecular scattering, must be subtracted to obtain b_{p550}. A more accurate writing of (9) should read

$$b_{p550}([\mathrm{Chl}]) = 0.30[\mathrm{Chl}]^{0.62} - b_{w\,550}. \qquad (9')$$

Even in the clearest waters, for example, when [Chl] = 0.02 mg m^{-3}, the molecular scattering represents about 7% (at 550 nm) of the total scattering coefficient; therefore this contribution is negligible considering the uncertainty attached to the above statistical relationship. The particle backscattering coefficient $b_{bp}(\lambda)$ is then obtained (as by JGR88) through the expression

$$b_{bp}(\lambda) = \{0.002 + 0.02[0.50 - 0.25 \log_{10}[\mathrm{Chl}]](550/\lambda)\}$$

$$\cdot \{b_{p\,550}([\mathrm{Chl}])\}. \qquad (10)$$

Note that the wavelength dependency λ^{-1} only applies to this part (within the brackets) of the backscattering efficiency (the embrace), which varies with [Chl].

Then $b_{bp}(\lambda)$ is added to $(1/2) b_w(\lambda)$, which represents the

backscattering coefficient of optically pure seawater, to obtain the total backscattering coefficient

$$b_b(\lambda) = (1/2)b_w(\lambda) + b_{bp}(\lambda). \tag{11}$$

Conversely to what happens for the total scattering coefficient, the molecular contribution is often important in forming the backscattering coefficient $b_b(\lambda)$; in effect, it becomes the dominant term at low chlorophyll concentration.

The previous $R(\lambda)$ values (reproduced from JGR88, Figure 13) are displayed in Figure 8a for comparison with the modified ones resulting from the introduction of the new set of $K_w(\lambda)$, $e(\lambda)$, and $\chi(\lambda)$ values. Both models are restricted to elastic scattering process; neither the Raman contribution (within the whole spectrum) nor the chlorophyll fluorescence contribution (around 683 nm) are accounted for. As expected from Figure 5, the differences between the two series of reflectance spectra essentially occur within the short wavelength domain (between 400 and 500 nm) and are increasingly significant when [Chl] decreases below 0.3 mg m^{-3}. This change mainly results from the change in the absorption coefficients for pure water. As a consequence of lower a_w values in this spectral domain, R reaches 10% around 420 nm, when [Chl] is 0.03 mg m^{-3} (instead of 6.5% with the previous model). Reflectance slightly exceeds 10% in the near-UV domain, around 370 nm, where the reflectance spectrum experiences its maximum (remember, however, that the e and χ parameters are somewhat uncertain in this domain). Interestingly, the shoulder in water absorption, at 450 nm, induces a noticeable inflexion in the $R(\lambda)$ spectrum, which logically develops when [Chl] decreases.

Besides the introduction of the new K_w, e, and χ values within the model, several other recent results or field data can be taken into consideration. Indeed, (9) can be replaced by a new empirical relationship, derived from a recent and much larger data set, and specifically valid for the oceanic upper layer [*Loisel and Morel*, 1998]; this revised expression, established for $\lambda = 660$ nm, is

$$b_{p660}([\text{Chl}]) = 0.347[\text{Chl}]^{0.766}$$

transformed into

$$b_{p550}([\text{Chl}]) = 0.416[\text{Chl}]^{0.766} \tag{12}$$

at 550 nm if a λ^{-1} spectral dependency is adopted for this scattering coefficient.

In addition, the particle backscattering coefficient will be modified in two ways. In (10) the backscattering efficiency for particles (described by the terms within the first embrace in this equation) was made of a constant background term (represented by 0.002) associated with a second one depending on the decimal logarithm of the chlorophyll concentration. Its maximal value was set to 0.02, when [Chl] = 0.01 mg m^{-3}, becoming zero when [Chl] = 100 mg m^{-3}. This varying term was made wavelength-dependent (through a λ^{-1} dependency) over the whole [Chl] domain. It is believed (see Figure 9) that the maximal backscattering efficiency value previously adopted (0.02) is too high for particles predominant in case 1 waters, presumed to be essentially biogenic. In fact, with a relative index of refraction likely to be close to 1.05 (on average) and sizes distributed according to Junge (power) laws with exponents close to -4, the backscattering efficiency cannot reach 2% (see also discussion by *Ulloa et al.* [1994]). Consequently, the maximal value of the backscattering efficiency is thus sim-

ply reset to 1% in (10). While a scattering spectral dependency expressed by λ^{-1} is typical of nonabsorbing particles distributed with a Junge exponent equal to -4, biogenic nonalgal particles in case 1 waters would exhibit a rather flat scattering (and backscattering) spectrum, essentially because they are increasingly absorbing in the short-wavelength domain, [see, e.g., *Bricaud et al.*, 1998]. For living algal cells, scattering spectra roughly mimic the absorption spectra but in a reverse manner [*Ahn et al.*, 1992]. This argument was used by *Gordon et al.* [1988] to parameterize the spectral backscattering coefficient as a function of increasing [Chl]. However, the very weak backscattering efficiency of algal cells [*Ahn et al.*, 1992] suggests that algae are hardly responsible for the formation of the backscattering coefficient.

There is an obvious contradiction here as algae cannot be responsible of the spectral behavior of the backscattering coefficient if, simultaneously, they are ineffective contributors to this coefficient. Perhaps the accompanying (detritic and others) minute particles, recognized to be the main contributors to backscattering, are "colored" enough to induce a spectral dependence of this coefficient. This question is still open and, as will be discussed later (Figure 15), the various parameterizations proposed to express the variation of b_b with [Chl] are highly diverging (and field determinations are obviously desirable).

The choice is made here to maintain the λ^{-1} dependency at the lower limit of the [Chl] range (namely, at 0.02 mg m^{-3}) when small detritus particles dominate and to diminish progressively this dependency according to the decimal logarithm of [Chl] in such a way that the backscattering becomes neutral (λ^0) at [Chl] = 2 mg m^{-3}. With both these modifications, (10) is transformed into

$$b_{bp}(\lambda) = \{0.002 + 0.01[0.50 - 0.25 \log_{10}[\text{Chl}]](\lambda/550)^v\}$$

$$\cdot \{b_{p\,550}([\text{Chl}])\}, \tag{13}$$

where the varying exponent v is expressed as

$$\begin{aligned} v &= (1/2)(\log_{10}[\text{Chl}] - 0.3), &&0.02 < [\text{Chl}] < 2 \text{ mg}^{-3}, \\ v &= 0, &&[\text{Chl}] \text{ is} > 2 \text{ mg m}^{-3}. \end{aligned} \tag{14}$$

Another small modification of the iterative scheme may also be introduced. The iterative process leading to the $R(\lambda)$ values, described above, makes use of a constant value (0.90) for the parameter μ_d (equations (8) and (8')). Actually, this average cosine, which is essentially governed by the Sun's position, also slightly varies along the spectrum and with the chlorophyll concentration [*Morel and Loisel*, 1998; *Loisel*, 1999]. This effect can tentatively be accounted for in a simplified manner by interpolating within lookup tables for this parameter for which the entries are λ, [Chl], and the zenith Sun angle in air, θ_s (example with $\theta_s = 30°$ shown in Table 3). The result of this modification is illustrated in Figure 8b, where θ_s is set equal to 30°.

The comparison between the solid curves in Figures 8a and 8b shows that with these modifications the computed reflectance values in the blue part of the spectrum ($\lambda < 500$ nm) are slightly increased at high chlorophyll concentration. For the red end of the spectrum (λ from about 600 to 700 nm) the new $R(\lambda)$ values, when compared to those in Figure 8a, are diminished for low [Chl], whereas they are raised at high [Chl] concentration. Also, the maximum, which develops at 565 nm when [Chl] increases, is somewhat sharper with the modified parameterization.
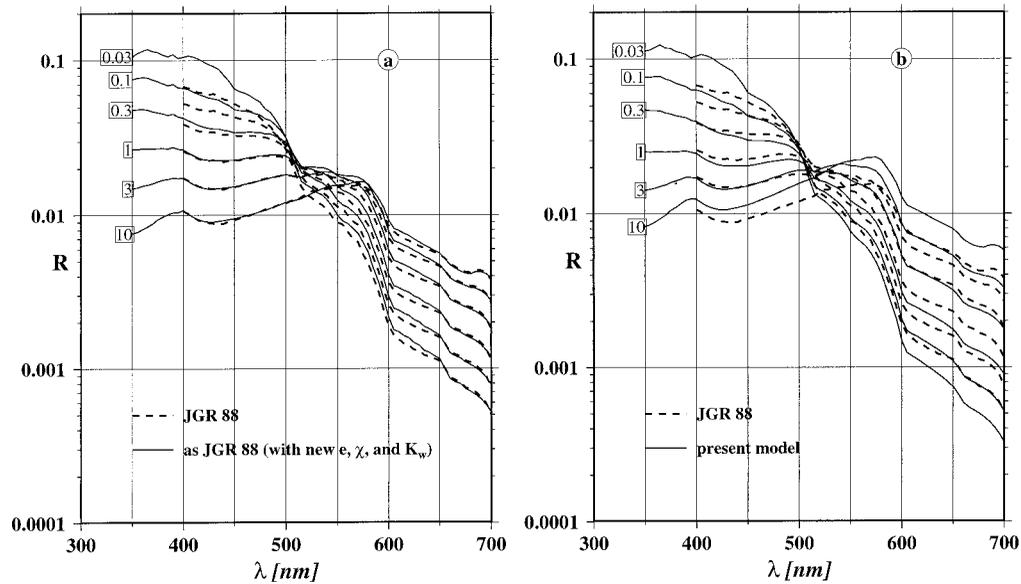
Figure 8. Modeled reflectance spectra for various chlorophyll concentration (mg m^{-3}), as indicated: (a) the solid curves (from 350 to 700 nm) are produced by introducing the new parameters, $e(\lambda)$, $\chi(\lambda)$, and $K_w(\lambda)$, within the unmodified JGR88 model and (b) the complete revised model (using (12), (13), and (14) and the varying μ_d values) is operated to draw the solid curves. In Figures 8a and 8b the dashed curves are reproduced from Figure 13 of JGR88.

The fact that the factor f (equation (7)) is maintained constant (0.33) has no significant impact on the shape of the modeled spectra. Indeed, f is weakly wavelength-dependent (by a few percent), while it is strongly Sun angle–dependent, between approximately 0.30 and 0.50 [see, e.g., *Morel and Gentili*, 1993, Figure 7]. As a consequence, accounting for the variations in f would result in a global shift of the spectra in Figure 8b without a significant effect upon their shape. As 0.33 represents a mean value valid when θ_s lies between 0 and 25°, an upward shift is to be expected for increasing θ_s values (for lower solar elevation).

3.5. Data and Model Comparison in Terms of Reflectance Spectra

It is worth recalling that in the development of the reflectance model the at-sea reflectance data themselves were never involved, so comparing them to the results from the model is in no way a circular argument. The reflectance spectra predicted by using the revised model account much better for in situ observations than did the former ones. This is demonstrated by Figure 10 where field data are displayed relative to ultraoligotrophic (Figure 10a) or moderately oligotrophic waters (Figure 10b). With [Chl] = 0.045 mg m^{-3} the experimental R spectra exhibit a flat maximum in the near-UV band, which tends to consolidate the model in this spectral domain, at least between 400 and 370 nm. The observed $R(\lambda)$ values (about 9%) in the violet part of the spectrum are well matched by the revised model (and revised absorption), while the 1988 model was unable to account for such high $R(\lambda)$ values. The inflexion at 450 nm predicted from the model is clearly detected in the field measurements. This feature indirectly confirms, via in situ determinations, the discovery by *Sogandares and Fry* [1997] and *Pope and Fry* [1997] of a shoulder in the pure water absorption spectrum at 450 nm. A similar observation can be made for the other set of spectra shown in Figure 10b, even if, with a higher

chlorophyll concentration the differences between the two models are lessening.

Although the new model generates lower $R(\lambda)$ at the long wavelengths (at least for [Chl] < 1 mg m^{-3}, Figure 8b), the previous examples (Figures 10a and 10b and many others not displayed) show that the predicted $R(\lambda)$ are often slightly above the observed values in the red part of the spectrum. This divergence in some way contradicts expectation. Indeed, to the extent that the Raman emission is not modeled the predicted R values actually are underestimated by about 8–10% (for very clear waters) within the blue-green spectral domain [*Stavn*, 1990; *Stavn and Weidemann*, 1992; *Gordon*, 1999] and even more (15%) in the long-wavelength range. Therefore it could have been anticipated that field data, in particular, in the red part of the spectrum, would stand above the predictions. The
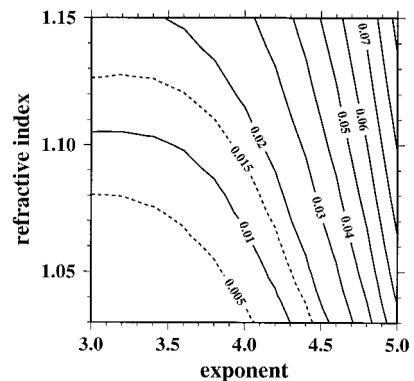

Figure 9. Backscattering efficiency $\bar{b}_b$ computed (via Mie theory) for populations of particles with a varying refractive index (relative to that of water) and a varying exponent of the Junge size distribution (with $n(D)$, the number of particles with a diameter D proportional to $D^{-\text{exponent}}$).

Table 3. Example, for a Sun Zenith Angle Equal to 30°, of a Simplified Table Giving the μ_d Values As a Function of the Wavelength and the Chlorophyll Concentration[a]

λ, nm	[Chl], mg m^{-3}				
	0.03	0.1	0.3	1	3
400	0.770	0.769	0.766	0.767	0.767
412	0.765	0.770	0.774	0.779	0.782
443	0.800	0.797	0.796	0.797	0.799
490	0.841	0.824	0.808	0.797	0.791
510	0.872	0.855	0.834	0.811	0.796
555	0.892	0.879	0.858	0.827	0.795
620	0.911	0.908	0.902	0.890	0.871
670	0.914	0.912	0.909	0.901	0.890

[a]See *Loisel* [1999] (also http://www.obs-vlfr.fr/~morel).

fact that the upward irradiances were measured at a nonzero (and varying) depth and were not successfully corrected for this effect partly explains this discrepancy and explains the increased dispersion of the spectra in this spectral domain. Self-shading by the instrument itself may also be responsible for these differences as it affects (decreases) the upwelling flux in a progressive manner toward the red end of the spectrum [*Gordon and Ding*, 1992]. It must be added that with the logarithmic scales and the span of the $R(\lambda)$ displayed in Figures 8 and 10 a 10% increase due to Raman effect remains hardly perceptible.

Expecting a total coincidence between actual and modeled spectra is illusory anyway; the natural variability in case 1 waters cannot be captured in a model based on average situation. Local and systematic nuances inside case 1 waters are detectable. For instance (Figure 10c), oligotrophic water reflectance spectra measured in three oceanic zones, with roughly similar low-chlorophyll contents, differ appreciably. A close look at the particle absorption spectra for these stations (data and Figure 2 by *Bricaud et al.* [1998]) also reveals differences that partly explain the observed divergence in $R(\lambda)$ in the short-wavelength (<450 nm) domain. Similar examples could be multiplied, for which the causes of deviation are sometimes identifiable (for instance, the dominance of a particular species, such as cyanobacteria [see *Morel*, 1997]), but more often, they remain unknown.

3.6. Data and Model Comparison in Terms of "Color Ratios"

The comparison between the previous (JGR88) model and the present one can be extended to the behavior of "blue-to-green" ratios, in other words, to the evolution of ratios of reflectances at 445 (or 490) and 555 nm along with the chlorophyll concentration. Such wavelengths and ratios are typically those used in the interpretation of remotely sensed ocean color data. The evolutions of the ratios $R(490)/R(555)$ and $R(443)/R(555)$, as produced by operating the reflectance model, are shown as solid curves in Figures 11a and 11b and are superimposed onto field data. The corresponding polynomials are given in Appendix A.

Compared to the predictions based on the previous JGR88 model, the revised model does a much better job in reproducing in a quantitative way the variation of these ratios with [Chl]. The improvement in the domain of low concentration mainly results from the use of lower water absorption values. For the $R(490)/R(555)$ ratio the agreement between modeled and field values is satisfactory, at least when comparing

the shape of the modeled curve and the general distribution of the data. In the 0.4–3 mg m^{-3} range, however, the measured ratios seem to be systematically above those predicted. This is not the case for the $R(443)/R(555)$ ratio, and the agreement is much better over almost the whole [Chl] range, except for the highest values, say above 4 or 5 mg m^{-3}. As the particle backscattering coefficient was made wavelength-independent within this concentration domain (equation (14)), the ratio of reflectances comes down to the inverted ratio of absorption, or as a proxy, to the inverted ratio of the attenuation coefficients (K). At very high [Chl], K_w becomes negligible compared to K_{bio}, so the asymptotic value of $R(443)/R(555)$ in the model reduces to the ratio $\chi(555)/\chi(443)$ (i.e., about 0.38) to the extent that the exponents at these two wavelengths are extremely close (0.642 versus 0.679, respectively). Actually, most of the present $R(445)/R(555)$ field data for high [Chl] are below this lower limit 0.38. When considering the Sea-viewing Wide Field-of-view (SeaWiFS) Bio-optical Algorithm Mini-Workshop (SeaBAM) data set [*O'Reilly et al.*, 1998] for high [Chl], the $R(445)/R(555)$ values, admittedly very scattered [see *O'Reilly et al.*, 1998, Figure 4], also tend to lie systematically below 0.38. In eutrophic waters, phytoplanktonic populations are generally dominated by large cells that exhibit a strong package effect. This effect leads to a reduction of the blue-to-green absorption ratio, in opposition to what would be necessary to explain the low values observed for the $R(445)/R(555)$ ratio. Therefore absorption does not seem to be involved; rather the way of modeling the spectral dependence of the backscattering coefficient for Chl-rich waters is likely not adequate and would be at the origin of the divergence. This remains an open question.

3.7. Additional Validation

The SeaBAM data set [*O'Reilly et al.*, 1998], containing coincident reflectance and chlorophyll measurements, can be used to test independently the present reflectance model. None of the reflectance measurements shown above (Figure 11) is included in the SeaBAM set. The original SeaBAM data set has been slightly reduced (from 919 to 865 stations) by eliminating data suspected to have been collected in case 2 waters (according to their geographical location) and also by excluding stations with [Chl] above 4 mg m^{-3} (actually, these two rejection criteria were largely coinciding).

The updated OC2 algorithm [*Maritorena and O'Reilly*, 2000], based on the $R(490)/R(555)$ ratio, is tuned to the SeaBAM data. An algorithm can be derived from the present model for the same band ratio (Figure 11a and polynomial in Appendix
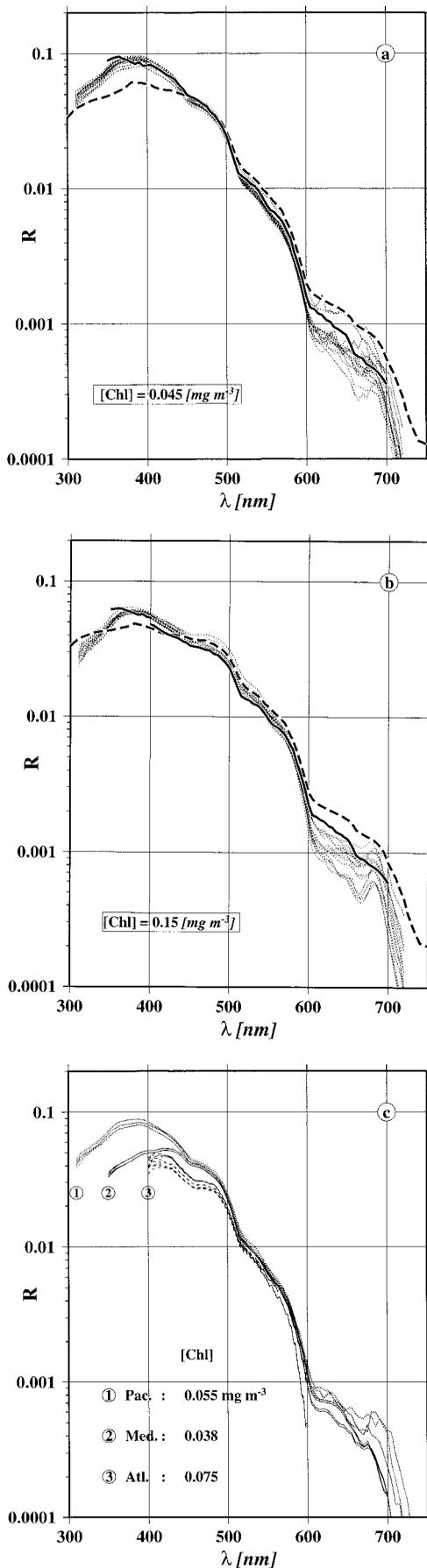
B). Both algorithms are simultaneously applied to the Sea-BAM data, and the corresponding [Chl] retrievals are displayed in Figure 12a in comparison with the sea-truth data. The "Morel-3" algorithm [*O'Reilly et al.*, 1998] (see also Appendix B) was based on the reflectances at 443 and 555 nm; this algorithm and the present algorithm (derived from the model and displayed in Figure 11b) are both operated, and the results are comparatively displayed in Figure 12b.

The gap in the data set for [Chl] values between 0.05 and 0.09 mg m^{-3} has no corresponding image in the histograms built with the retrieved data, whatever the algorithms and wavelengths considered. With the present reflectance model there is a definite advantage in using the second couple of wavelengths (443–555 nm), more appropriate particularly for the low [Chl] values (as noted before when discussing Figure 11a, an underestimate of [Chl] is to be expected from the use of the modeled $R(490)/R(555)$ ratio); even near the upper limit of the Chl range, the use of the $R(443)/R(555)$ model remains efficient. Actually, the agreement between the retrievals through the updated OC2 and through the present model operated with the $R(443)/R(555)$ ratio is worth being noted.

The purpose at this point is not to discuss the skill of algorithms. The aim of this test is rather to examine whether the bio-optical model proposed here, from which the reflectance model derives, has a general applicability in other oceanic zones. On average, the model is able to account for observations in diversified case 1 waters and at this stage can be considered as validated, within the variability expected in case 1 waters.

4. Discussion and Conclusion

There is not a unique way of building a "bio-optical model" of oceanic case 1 water, and this point deserves examination and arises several questions. For instance, is the present analysis, and subsequent optical modeling based on K_d, consistent with other approaches based on the absorption coefficient? What is the extent of the optical properties variability in case 1 water, and can the source of this variability be identified? What are the main weaknesses, or lack of knowledge, if one tries to develop a purely analytical method (based on the IOP of optically significant constituents) with the purpose of pre-

Figure 10. (opposite) Comparison between modeled reflectance spectra (logarithmic scale) and spectra measured (dotted curves) in two locations in tropical Pacific: (a) at 150°W, 16°S (November 25–27, 1994) and (b) at 150°W, 5°S (November 18–22, 1994). The dashed curves come from the JGR88 model, and the solid curves come from the presently revised model. During the 5 days in each location (dotted reflectance spectra) the chlorophyll concentration was rather steady, varying between 0.042 and 0.058 (average 0.045 mg m^{-3} at 16°S) and 0.144 and 0.179 (average 0.150 mg m^{-3} at 5°S). Note that the Chl fluorescence emission around 685 nm (not modeled) is clearly detected when [Chl] is 0.15 mg m^{-3} (Figure 10b). (c) Reflectance spectra (several determinations) in three locations, namely, in the Pacific Ocean (150°W, 16°S, November 28, 1994; OLIPAC), in the Atlantic Ocean (31°W, 21°N, October 20, 1991; EUMELI 3), and in the Mediterranean Sea (MINOS, June 9, 1996; 32°E, 34°N); the chlorophyll concentrations as indicated are mean values computed for the upper (0–15 m) layer at each station.

dicting apparent optical properties and spectral reflectance in particular?

4.1. Diffuse Attenuation-Based Versus Absorption-Based Models

The spectral absorption by suspended (algal and nonalgal) particles, denoted $a_p(\lambda)$, has been recently studied in various oceanic waters [Bricaud et al., 1998], and its variations have been empirically related to [Chl] through nonlinear relationships:

$$a_p(\lambda) = A(\lambda)[Chl]^{E(\lambda)}. \quad (15)$$

The statistical relationship between the particle scattering coefficient b_p (at 660 nm) and [Chl] in case 1 waters has also been reinvestigated [Loisel and Morel, 1998, equation (11)]. By using these recent formulations to get the absorption and scattering coefficients, a and b, and combining them in Kirk's [1981] formula it is possible to reconstruct the diffuse attenuation coefficient $K_d(\lambda)$ as a function of the chlorophyll concentration. The comparison between these reconstructions of $K_d(\lambda)$ and the present results (referred to as "in preparation" by Bricaud et al. [1998]) has already been presented [Bricaud et al., 1998, Figure 6]. The agreement between the two approaches, over 2 orders of magnitude in K_{bio} and in [Chl], is very good considering that the data sets largely differ in their geographical origin and, more importantly, that the involved methodologies are totally independent.

Indeed, $K_d(\lambda)$ is derived from in situ measurements and thus cumulates the effects of all kinds of absorbing and scattering materials present in the water column. In contrast, the absorption coefficient of particulate matter is determined on discrete samples by using an in vitro filter technique. The reconstruction of $K_d(\lambda)$ implies the use of the relationship between b_p and [Chl] (mentioned above). More problematic is the hypothesis about the amount of dissolved yellow substance, generally not determined. The required assumption when reconstructing $K_d(\lambda)$ consists of adopting a relationship between the amount of local yellow substance (YS) and the chlorophyll concentration. It is worth noting that the assumption concerning the spectral shape of the YS absorption is less crucial to the extent that its exponential increase toward the short wavelengths and the corresponding slope are well known and rather constant features. Results by Bricaud et al. [1998, Figure 6] (for [Chl] = 0.1, 1, and 10 mg m^{-3}) suggest that in case 1 waters the ratio between YS absorption (at 440 nm) and water plus particles (algal and nonalgal) absorption at the same wavelength might be about 20% when [Chl] = 0.1 mg m^{-3} and that this ratio would increase for increasing chlorophyll concentration [see also Siegel and Michaels, 1996; Nelson et al., 1998].

The comparison between the two approaches can be made the other way around as a cross check. Indeed, the K coefficients can be transformed into absorption coefficients by using the iterative procedures that have led to the reflectance model (namely, (8), (8′), and (8″)). The results of such an "inversion" procedure are displayed in Figure 13 for three chlorophyll values. Also shown are the spectra directly produced by the particle absorption model of Bricaud et al. [1998], with a constant contribution of YS absorption set at 20% of the water plus particle absorption. In addition, the spectra resulting from another parameterization, derived from Prieur and Sathyendranath [1981] and used by Morel [1991, equations (20a) and (20b)] are drawn (it must be noted that equations (20a) and
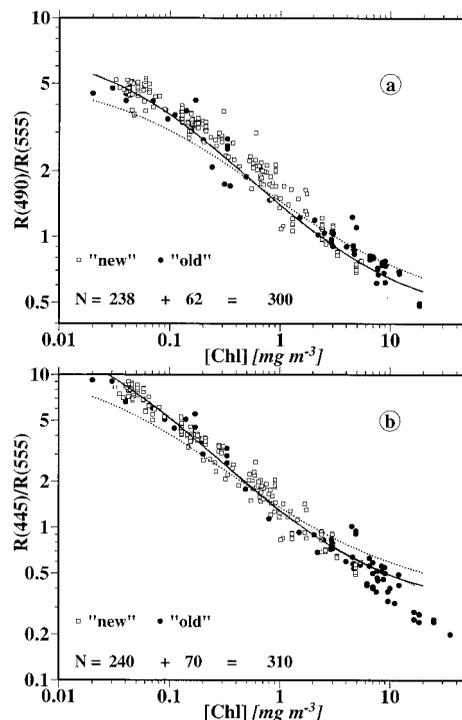

Figure 11. Ratios of reflectance values for the wavelengths (a) 490 and 555 nm and (b) 445 and 555 nm plotted as a function of the chlorophyll concentration; both scales are logarithmic. The old and new data (see text) are shown with distinct symbols. The dashed curves represent the prediction based on the previous model (JGR88), whereas the solid curves are for the present model (and use the wavelengths 443, 490, and 555).

(20b), incorrectly written by Morel [1991], are corrected in Appendix B).

Actually, the three ways of modeling the spectral absorption as a function of the chlorophyll concentration lead to results that are rather close together, although some systematic discrepancies exist in the blue part of the spectrum in particular (Figure 13). It must be realized that the observed differences are actually inferior to the confidence intervals attached to each approach (and to the uncertainties attached to subsequent parameterization). By recalling that each model is based on mean values that result from statistical analyses of differing data sets it is not surprising that they do not exactly coincide. The direct model, based on $a_p(\lambda)$, tends to provide absorption values lower than those derived from the use of $K_d(\lambda)$, as soon as [Chl] exceeds 0.1 mg m^{-3}. This increasing deviation again suggests that the constant ratio (20%) depicting the absorption contribution of YS must be made more realistically varying and dependent on [Chl], even if a simple proportionality is not to be expected [Bricaud et al., 1981]. Simultaneous YS absorption and [Chl] determinations in case 1 waters remain presently rather scarce; therefore parameterizing the YS contribution to absorption remains presently uncertain.

The rather large deviations of actual $a_p(\lambda)$ values from their mean value were analyzed by Bricaud et al. [1998]. Bricaud et al. [1998, Figure 9] showed that these deviations for two wavelengths (λ = 440 and 550 nm, taken as examples) are positively correlated. A similar analysis can be performed with respect to K_{bio} by forming the relative deviation (%) between the mea-
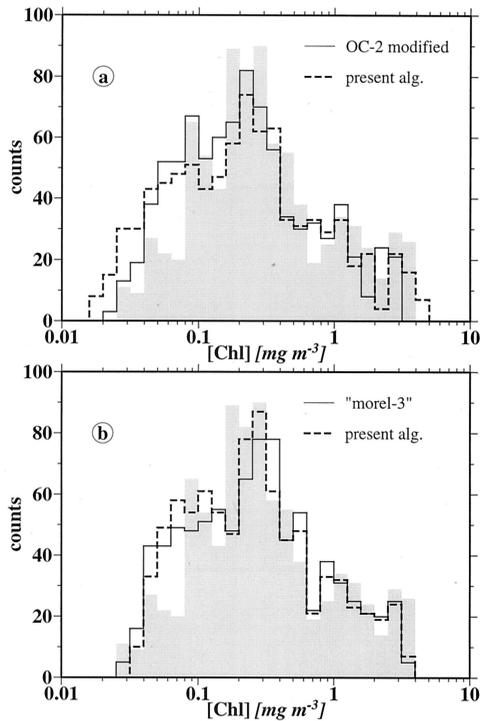
Figure 12. The shaded area represents the frequency distribution of [Chl] in the SeaBAM data set. (a) The [Chl] retrievals when using the wavelengths 490 and 555 nm and two different algorithms (see text) are shown as solid or dashed histograms. (b) The same as Figure 12a but when 443 and 555 nm are used. In abcissae the increment in [Chl] corresponds to 10 logarithmically equal classes per decade.

sured K_{bio} values and those predicted through (5) from the actual chlorophyll concentration:

$$\delta K_{\mathrm{bio}} = 100(\text{measured } K_{\mathrm{bio}} - \text{predicted } K_{\mathrm{bio}})/\text{predicted } K_{\mathrm{bio}}.$$

This analysis (Figure 14 provides an example) leads to a conclusion similar to that drawn for $a_p(\lambda)$; the deviations (δK_{bio}) at the two wavelengths 490 and 555 nm are generally concomitant. In other words, the variability in a_p or in K_{bio} affects more the magnitude of these coefficients than the shape of the corresponding spectra.

There are no convincing arguments to select one approach rather than another when modeling the absorption coefficient in case 1 waters. The bio-optical model of absorption, based on the use of the a_p statistical analysis [*Bricaud et al.*, 1998], is in essence the most direct. Nonetheless, in the absence of a reliable relationship between YS absorption and [Chl] content it cannot properly account for the influence of colored dissolved organic matter. Any possible influence of tiny colored particles, not retained by filtration, also remains ignored. The differences in shape of the reconstructed K_{bio} spectra [*Bricaud et al.*, 1998, Figure 6], or the differences in absorption spectra shown in Figure 13, likely originate from these weaknesses, which particularly affect the blue part of the spectrum.

Such drawbacks do not exist for $K_d(\lambda)$, which collectively accounts for all dissolved and suspended materials; some uncertainties, however, may occur in the red part of the spectrum if the K_d value has been depressed by the effect of Raman scattering. Apart from this possible flaw, there are some advantages in measuring and using $K_d(\lambda)$. Indeed, there is a

minimum of experimental errors because, first, the irradiance measurements are not intrusive and, second, the absolute radiometric calibration of the instrument is not involved (equation (1)); the same can be said for $R(\lambda)$ as long as a unique collector is used to measure the upwelling and downwelling light fluxes; see (2)). However, if the purpose is to retrieve indirectly and then study absorption, the accurate derivation of this coefficient is not straightforward. The extraction of $a(\lambda)$ from the diffuse attenuation involves the manipulation of the radiative transfer equation, here treated in a simplified manner. More rigorous inversions of this equation are available. They require the knowledge of the actual volume scattering function and must take into consideration the illumination regime above the surface as boundary conditions. This is the right approach to employ when the determination of all the needed properties will be accurate enough to justify such rigorous computations.

4.2. Toward an Analytical Reflectance Model?

Any analytical reflectance model for case 1 waters ideally would rest on the prediction as a function of [Chl] of the IOPs, namely, a, b, and the phase function, in view of forming ratios like $b_b/(a + b_b)$ or b_b/a. The Sun angle– and sky-dependent factors (the f factors), which relate R to the two ratios above, are out of the scope of the present discussion, as is the bidirectional radiance field structure [see *Morel and Gentili*, 1993, 1996]. When (given the IOPs) the radiative transfer equation is accurately solved, the f factors and bidirectional functions are numerically determined so that R can be "analytically" modeled in all illumination conditions.

Therefore such a purely analytical approach, within reach from a computational viewpoint, implies that each of the two needed coefficients, a and b_b (or, better, the volume scattering function), is reconstructed as the sum of the separate contributions of all significant constituents. These contributions must be known and expressed as a function of [Chl] when formulating the case 1 water reflectance model. Considering, first, absorption, as said above, the first way of modeling this coef-
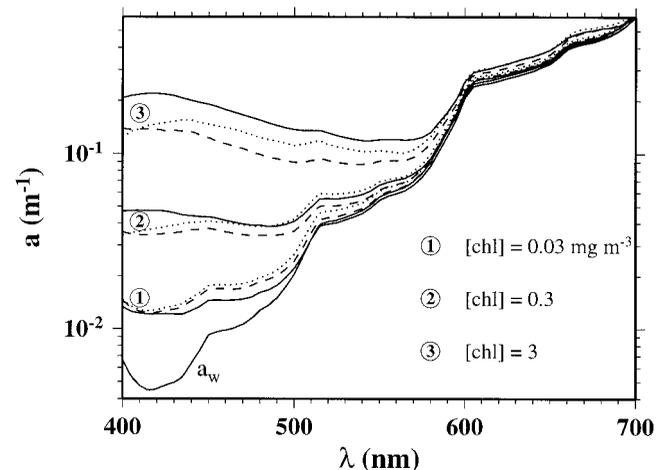

Figure 13. Absorption spectra for three [Chl] values reconstructed by using three different models (see text); the dashed curves are produced by using (15), the dotted curves are produced by using (16) (Appendix B), and the solid curves are produced by using the iterative procedure (equations (8), (8'), and (8'')). The absorption spectrum of pure water, a_w [*Pope and Fry*, 1997], is also displayed.

ficient (via a_p) is direct, but some of the constituents are not described, and thus hypotheses are needed; the second way (via K_d) accounts for all the contributors to absorption, yet it cannot be qualified as truly analytical to the extent that K_d is not an IOP.

Now, the way of modeling b_b remains to be examined. It generally requires two steps. First, the scattering coefficient is related to the chlorophyll concentration (e.g., (12)), which actually is an empirical relationship); then, a value for the backscattering efficiency (the ratio b_{bp}-to-b_p, denoted $\tilde{b}_b$) must be adopted. Concerning the first step, data are available to document the b_p-[Chl] relationship. It must be emphasized, however, that the dispersion in this natural relationship is definitely large [*Gordon and Morel*, 1983] and was not reduced when supposedly more accurate data were examined [*Loisel and Morel*, 1998]. Concerning the second step, expressing $\tilde{b}_b$ implies three kinds of assumptions, about its own magnitude, about its variation along with the chlorophyll concentration, and about its wavelength dependence (e.g., (10) or (13)). It is worth recalling that in general, the spectral behavior of the scattering and backscattering coefficients is not necessarily the same [*Morel and Bricaud*, 1981]. For algal cells the depressive effect of absorption is generally more marked on b_b than on b [*Ahn et al.*, 1992]. This additional complexity, which is well understood from a theoretical viewpoint, is not practically predictable and parameterized in a safe manner.

So far, there is no information about the existence in case 1 waters of a reliable relationship between b_{bp} and [Chl], and more generally, it could be said that the backscattering properties of oceanic particles remain poorly known. This lack of knowledge has been circumvented by "reasonable" hypotheses about $\tilde{b}_b$ based on theoretical considerations that involve the size distribution and the composition (index of refraction) of the particulate matter in oceanic waters (e.g., (13) replacing (10)). Various formulations of this nature have been proposed and are comparatively summarized below.

A classical approach, in particular, in radiative transfer modeling, has consisted of using a unique (assumed to be typical) particle phase function derived from Petzold's data [see *Mobley*, 1994]. The adoption of this unique phase function was also made for the sake of numerical convenience in intercomparison exercises of radiative transfer models [e.g., *Mobley et al.*, 1993]. The backscattering efficiency, which results from the shape of the Petzold's function, gets up to 1.9%. When such an efficiency is combined with the b_p value that results from the b_p-[Chl] relationship, uncomfortably high backscattering coefficients (and reflectances) are obtained as soon as [Chl] exceeds about 1 mg m^{-3} (see Figure 15a). This limitation, already discussed when producing the f factors and bidirectional functions [*Morel and Gentili*, 1991, 1996], definitely impedes a realistic reflectance model based on this unique $\tilde{b}_b$ value to be developed.

Theoretical considerations and experiments have shown that the backscattering efficiency of algal cells is extremely low [*Morel and Bricaud*, 1981; *Ahn et al.*, 1992]. It has also been demonstrated [*Stramski and Kiefer*, 1991; *Morel and Ahn*, 1991] that for oceanic waters the values of the backscattering coefficients, needed to account for the observed reflectance, cannot be attributed to well-identified particles, such as algal cells and heterotrophic bacteria. It must, rather, be admitted that the bulk of the backscattering is essentially ensured by extremely small (<0.5 μm) and largely unidentified particles; bubbles may also play a role in this process [*Stramski*, 1994; *Zhang et*
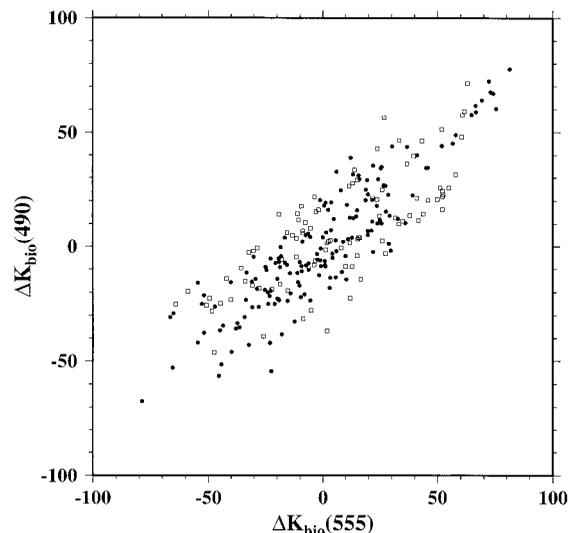

Figure 14. Relative deviations of the actual K_{bio} values from their mean values computed via (5). The relative deviations at wavelength 490 nm are plotted versus those at 555 nm.

al., 1998]. In this respect the spectral volume scattering function model for particles, proposed by *Kopelevich* [1983] and extended by *Haltrin and Kattawar* [1991], separates the contributions by small, refringent, supposedly mineral particles and by large and soft biological particles. The backscattering probabilities are 3.9 and 0.064% for the small and large particles populations, respectively. The fact that b_b remains low (Figure 15a) despite the high $\tilde{b}_b$ value attributed to small particles originates from the relationship between b and [Chl] [see *Mobley*, 1994, equation (3.43) and Table 1], which leads to b values about 3 times less than those provided by (12).

Anyway, this two-component model, or several others like the one represented by (10) (modified in (13)) or the one proposed by *Gordon et al.* [1988; see also *Gregg et al.*, 1993, Table 3], remains to be validated via experiments. In summary, not only the parameterization of b_b in terms of chlorophyll concentration is far from being ascertained but also the various expressions presently in use diverge significantly; this is amply demonstrated by Figure 15a, dealing with the wavelength 443 nm and several proposed parameterizations, as well by Figure 15b, dealing with the spectral dependence of b_b and various [Chl]. There is no point in commenting on these differences without new decisive arguments or experimental determinations. Although the protocols and methodologies are evolving and measurements are now possible [*Maffione and Honey*, 1992; *Maffione and Dana*, 1997], results remain scarce [see *Stramski et al.*, 1999].

To the question used as title for this paragraph it could be answered that presently, an analytical approach is not within easy reach as the IOPs of the constituents, or the bulk IOPs, remain insufficiently known. Therefore it is still necessary to rely on empirical or semianalytical models, which can certainly be improved. The possible variations of the ratio between nonalgal and algal absorption and between dissolved and particulate matter absorption and, more importantly, the present lack of knowledge about the possible change of the particle phase function with [Chl] remain considerable obstacles when trying to predict the AOPs. This weakness is particularly crucial for the prediction of the reflectance magnitude, as well as
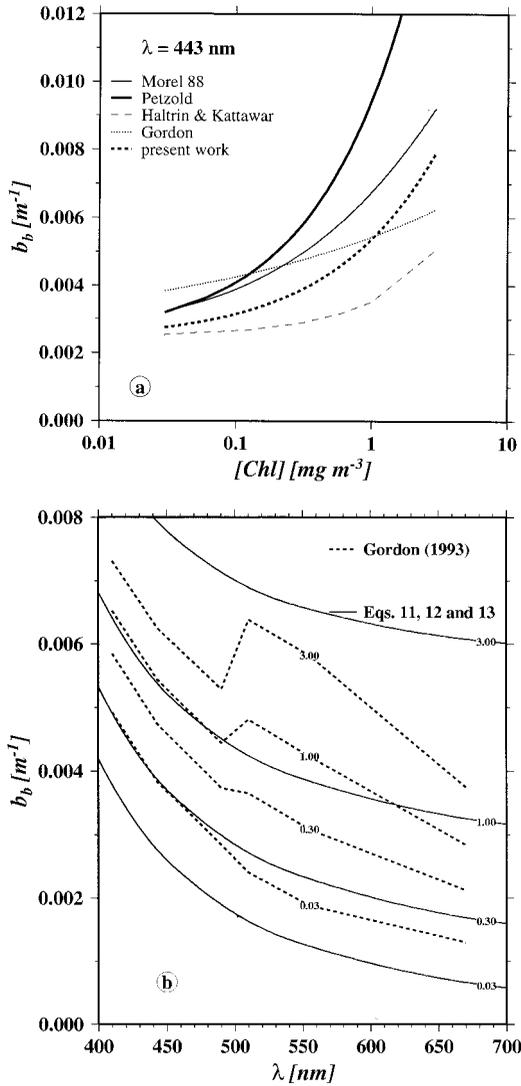
Figure 15. (a) Evolution of the backscattering coefficient at 443 nm with [Chl], according to various parameterizations [*Gordon et al.*, 1988; *Haltrin and Kattawar*, 1991; JGR88] (see also Petzold's phase function used in conjunction with (9)). (b) Spectral b_b values for various [Chl], according to *Gordon* [1993] (tabulated by *Gregg et al.* [1993]) and (11), (12), and (13).

for the prediction of the bidirectional properties of the upward radiance field, which heavily depend on the shape of the backward lobe of the phase function.

Ratios of reflectances at two wavelengths are more predictable than single (monochromatic) reflectance. Indeed, such ratios are less affected by uncertainties attached to b_b for particles and are, in general, less sensitive to the natural variability of IOPs owing to the existence of spectral covariances. This conjecture is supported by the good agreement between modeled and actual evolutions of reflectance ratios with [Chl], as demonstrated by Figure 11. In the domain of low [Chl], when molecular scattering dominates the backscattering process and thus when particle backscattering plays a minor role, the good agreement is not surprising, especially if the absorption values for pure water are accurately represented, as they seem to be when *Pope and Fry*'s [1997] values are adopted. In the domain of high [Chl], when the role of molecular scattering

and absorption is reduced, the agreement deteriorates, the variability of the optical properties increases, and a ubiquitous model for case 1 waters based on global relationships becomes less and less accurate. Models of more restricted (geographically and seasonally) applicability, perhaps of higher complexity, and forming a transition with models developed for case 2 waters, will be revealed to be more efficient in productive case 1 waters.

Appendix A

The analytically modeled ratios of reflectances at two wavelengths λ_1 and λ_2, such as those represented as solid curves in Figure 11, can be expressed through cubic polynomials of the general form

$$\log [\text{Chl}] = a_0 + a_1 R + a_2 R^2 + a_3 R^3,$$

where $R = \log [R(\lambda_1)/R(\lambda_2)]$ and where "log" symbolizes decimal logarithm. The coefficients are as follows: for $\lambda_1 = 490$ and $\lambda_2 = 555$ nm, $a_0 = 0.3603$, $a_1 = -2.8231$, $a_2 = 2.3835$, and $a_3 = -3.0930$, and for $\lambda_1 = 443$ and $\lambda_2 = 555$ nm, $a_0 = 0.20696$, $a_1 = -2.0952$, $a_2 = 1.25708$, and $a_3 = -0.9376$. The semianalytical algorithm making use of the 443 and 555 nm wavelengths and called the Morel-3 algorithm by *O'Reilly et al.* [1998] is a previous version of the present one; it is represented by the modified model displayed in Figure 8a (denoted JGR88 model, with the new spectral values for K_w, e, and χ).

Appendix B

The relationship between the spectral values of the absorption coefficient and the chlorophyll concentration, which accounts for the effect of a covarying amount of dissolved YS, was mistakenly expressed through only two equations by *Morel* [1991, equations (20a) and (20b)] and repeated by *Morel and Gentili* [1991, equations (8) and (9)] and elsewhere. The correct computations, which include three successive steps, must be expressed by the set of the three following equations:

$$a(\lambda) = a_w(\lambda) + 0.06 A_{\text{chl}}(\lambda)(\text{Chl})^{0.65} + a_y(\lambda), \quad (16)$$

where

$$a_y(\lambda) = a_y(440) \exp [-0.014(\lambda - 440)] \quad (17)$$

$$a_y(440) = 0.2[a_w(440) + 0.06 A_{\text{chl}}(440)(\text{Chl})^{0.65}], \quad (18)$$

where the coefficient $A_{\text{chl}}(440)$ is unity in (18). *Bricaud et al.* [1981, equation (17)] express the exponential decrease of the YS absorption a_y for increasing wavelength; the particular value of this coefficient at wavelength 440 nm, $a_y(440)$, is taken [*Prieur and Sathyendranath*, 1981, equation (18)] as a constant fraction (0.2) of the absorption due to both water and algal material. Therefore this expression does not reduce to pure water absorption even if the chlorophyll concentration is zero, as a background will remain. This choice is obviously debatable, as the choice of a constant proportionality expressed by the factor 0.2 [see *Bricaud et al.*, 1998]. If this factor becomes a free parameter, the above two-component model would change into a "three-component" model.

References

Ahn, Y.-H., A. Bricaud, and A. Morel, Light backscattering efficiency and related properties of some phytoplankters, *Deep Sea Res.*, *Part A*, *39*, 1835–1855, 1992.

Baker, K. S., and R. C. Smith, Bio-optical classification and model of natural waters, II, *Limnol. Oceanogr.*, *27*, 500–509, 1982.

Boivin, L. P., W. F. Davidson, R. S. Storey, D. Sinclair, and E. D. Earle, Determination of the attenuation coefficient of visible and ultraviolet radiation in heavy water, *Appl. Opt.*, *25*, 188–192, 1986.

Bricaud, A., A. Morel, and L. Prieur, Absorption by dissolved organic matter of the sea (yellow substance) in the UV and visible domains, *Limnol. Oceanogr.*, *26*, 43–53, 1981.

Bricaud, A., A. Morel, M. Babin, K. Allali, and H. Claustre, Variations of light absorption by suspended particles with chlorophyll *a* concentration in oceanic (case 1 waters): Analysis and implications for bio-optical models, *J. Geophys. Res.*, *103*, 31,033–31,044, 1998.

Claustre, H., Phytoplankton pigment signatures of the trophic status in various oceanic regimes, *Limnol. Oceanogr.*, *39*, 1207–1211, 1994.

Garver, S., D. A. Siegel, and B. G. Mitchell, Variability in near-surface particulate absorption spectra: What can a satellite ocean color imager see?, *Limnol. Oceanogr.*, *39*, 1349–1367, 1994.

Gibbs, C. F., Chlorophyll *b* interference in the fluorimetric determination of chlorophyll *a* and phaeopigments, *Aust. J. Mar. Freshwater Res.*, *30*, 597–606, 1979.

Gordon, H. R., Dependence of the diffuse reflectance of natural waters on the Sun angle, *Limnol. Oceanogr.*, *34*, 1484–1489, 1989.

Gordon, H. R., Contribution of Raman scattering to water-leaving radiance: A reexamination, *Appl. Opt.*, *38*, 3166–3174, 1999.

Gordon, H. R., and K. Ding, Self-shading of in-water optical instruments, *Limnol. Oceanogr.*, *37*, 491–500, 1992.

Gordon, H. R., and W. R. McCluney, Estimation of the depth of Sun light penetration in the sea for remote sensing, *Appl. Opt.*, *14*, 413–416, 1975.

Gordon, H. R., and A. Morel, Remote assessment of ocean color for interpretation of satellite visible imagery: A review, 114 pp., Springer-Verlag, New York, 1983.

Gordon, H. R., O. B. Brown, and M. M. Jacobs, Computed relationships between inherent and apparent optical properties of a flat homogeneous ocean, *Appl. Opt.*, *14*, 417–427, 1975.

Gordon, H. R., O. B. Brown, R. H. Evans, J. W. Brown, R. C. Smith, K. S. Baker, and D. K. Clark, A semianalytical radiance model of ocean color, *J. Geophys. Res.*, *93*, 10,909–10,924, 1988.

Gregg, W. W., F. C. Chen, A. L. Mezaache, J. D. Chen, and J. F. Whiting, The simulated SeaWiFS data set, version 1, in *SeaWiFS Technical Report Series*, vol. 9, edited by S. B. Hooker, *NASA Tech. Memo. 1999-206892*, pp. 1–17, Goddard Space Flight Cent., Greenbelt, Md., 1993.

Haltrin, V. I., and G. Kattawar, Light fields with Raman scattering and fluorescence in sea water, technical report, 74 pp., Dep. of Phys., Texas A&M Univ., College Station, 1991.

Kirk, J. T. O., A Monte Carlo study of the nature of the underwater light field in, and the relationships between optical properties of, turbid yellow waters, *Aust. J. Mar. Freshwater Res.*, *32*, 517–532, 1981.

Kirk, J. T. O., Dependence of relationship between inherent and apparent optical properties of water on solar altitude, *Limnol. Oceanogr.*, *29*, 350–356, 1984.

Kopelevich, O. V., Small-parameter model of optical properties of sea water (in Russian), in *Ocean Optics*, vol. I, *Physical Ocean Optics*, edited by A. S. Monin, chap. 8, pp. 208–234, Nauka, Moscow, 1983.

Loisel, H., Contribution à l'étude des propriétés bio-optiques et du transfert radiatif dans l'océan: Applications, Ph.D. thesis, 168 pp., Université Pierre et Marie Curie, Paris, 1999.

Loisel, H., and A. Morel, Light scattering and chlorophyll concentration in case 1 waters: A reexamination, *Limnol. Oceanogr.*, *43*, 847–858, 1998.

Maffione, R. A., and D. R. Dana, Instruments and methods for measuring the backward scattering coefficient of ocean waters, *Appl. Opt.*, *36*, 6057–6067, 1997.

Maffione, R. A., and R. C. Honey, Instrument for measuring the volume scattering function in the backward direction, *Proc. SPIE Opt. Eng.*, *1750*, 15–26, 1992.

Maritorena, S., and J. O'Reilly, Update on the initial operational SeaWiFS chlorophyll *a* algorithm, in *SeaWiFS Postlaunch Technical Report Series*, vol. 11, edited by S. B. Hooker and E. R. Firestone, *NASA Tech. Memo. 1999-206892*, pp. 3–8, Goddard Space Flight Cent., Greenbelt, Md., 2000.

Mitchell, B. G., and O. Holm-Hansen, Bio-optical properties of Antarctic Peninsula waters: Differentiation from temperate ocean models, *Deep Sea Res.*, *Part A*, *38*, 1009–1028, 1991.

Mobley, C. D., *Light and Water: Radiative Transfer in Natural Waters*, 592 pp., Academic, San Diego, Calif., 1994.

Mobley, C. D., B. Gentili, H. R. Gordon, Z. Jin, G. W. Kattawar, A. Morel, P. Reinersman, K. Stamnes, and R. H. Stavn, Comparison of numerical models for computing underwater light fields, *Appl. Opt.*, *32*, 7484–7505, 1993.

Morel, A., Optical modeling of the upper ocean in relation to its biogenous matter content (case 1 waters), *J. Geophys. Res.*, *93*, 10,749–10,768, 1988.

Morel, A., Light and marine photosynthesis: A spectral model with geochemical and climatological implications, *Prog. Oceanogr.*, *26*, 263–306, 1991.

Morel, A., Consequences of a *Synechococcus* bloom upon the optical properties of oceanic (case 1) waters, *Limnol. Oceanogr.*, *42*, 1746–1754, 1997.

Morel, A., and Y. H. Ahn, Optics of heterotrophic nanoflagellates and ciliates: A tentative assessment of their scattering role in oceanic waters compared to those of bacterial and algal cells, *J. Mar. Res.*, *49*, 177–202, 1991.

Morel, A., and D. Antoine, Heating rate within the upper ocean in relation to its bio-optical state, *J. Phys. Oceanogr.*, *24*, 1652–1665, 1994.

Morel, A., and J.-F. Berthon, Surface pigments, algal biomass profiles, and potential production of the euphotic layer: Relationships reinvestigated in view of remote sensing applications, *Limnol. Oceanogr.*, *34*, 1545–1562, 1989.

Morel, A., and A. Bricaud, Theoretical results concerning light absorption in a discrete medium, and application to specific absorption of phytoplankton, *Deep Sea Res.*, *Part A*, *28*, 1375–1393, 1981.

Morel, A., and B. Gentili, Diffuse reflectance of oceanic waters: Its dependence on Sun angle as influenced by the molecular scattering contribution, *Appl. Opt.*, *30*, 4427–4438, 1991.

Morel, A., and B. Gentili, Diffuse reflectance of oceanic waters, II, Bi-directional aspects, *Appl. Opt.*, *32*, 6864–6879, 1993.

Morel, A., and B. Gentili, Diffuse reflectance of oceanic waters, III, Implication of bidirectionality for the remote-sensing problem, *Appl. Opt.*, *35*, 4850–4862, 1996.

Morel, A., and H. Loisel, Apparent optical properties of oceanic water: Dependence on the molecular scattering contribution, *Appl. Opt.*, *37*, 4765–4776, 1998.

Morel, A., and L. Prieur, Analysis of variations in ocean color, *Limnol. Oceanogr.*, *22*, 709–722, 1977.

Nelson, N. B., D. A. Siegel, and A. F. Michaels, Seasonal dynamics of colored dissolved material in the Sargasso Sea, *Deep Sea Res.*, *Part I*, *45*, 931–957, 1998.

O'Reilly, J. E., S. Maritorena, B. G. Mitchell, D. A. Siegel, K. L. Carder, S. A. Garver, M. Kahru, and C. McClain, Ocean color chlorophyll algorithms for SeaWiFS, *J. Geophys. Res.*, *103*, 24,937–24,953, 1998.

Pope, R. M., and E. S. Fry, Absorption spectrum (380–700 nm) of pure water, II, Integrating cavity measurements, *Appl. Opt.*, *36*, 8710–8723, 1997.

Preisendorfer, R. W., Application of radiative transfer theory to light measurements in the sea, *IUGG Monogr.*, *10*, 11–30, 1961.

Prieur, L., Transfert radiatif dans les eaux de mer, D.Sc. thesis, Pierre et Marie Curie Univ., Paris, 1976.

Prieur, L., and S. Sathyendranath, An optical classification of coastal and oceanic waters based on the specific absorption curves of phytoplankton pigments, dissolved organic matter, and other particulate materials, *Limnol. Oceanogr.*, *26*, 671–689, 1981.

Quickenden, T. I., and J. A. Irvin, The ultraviolet absorption of liquid water, *J. Chem. Phys.*, *72*, 4416–4428, 1980.

Siegel, D. A., and A. F. Michaels, Quantification of non-algal light attenuation in the Sargasso Sea: Implications for biogeochemistry and remote sensing, *Deep Sea Res.*, *Part II*, *43*, 321–345, 1996.

Smith, R. C., and K. S. Baker, Optical properties of the clearest natural waters (200–800 nm), *Appl. Opt.*, *20*, 177–184, 1981.

Sogandares, F. M., and E. S. Fry, Absorption spectrum (340–640 nm)

of pure water, I, Photothermal measurements, *Appl. Opt.*, *33*, 8699–8709, 1997.

Stavn, R. H., Raman scattering effects at the shorter visible wavelengths in clear ocean waters, *Proc. SPIE Int. Soc. Opt. Eng.*, *1302*, 94–100, 1990.

Stavn, R. H., and A. D. Weidemann, Raman scattering in ocean optics: Quantitative assessment of internal radiant emission, *Appl. Opt.*, *31*, 1294–1303, 1992.

Stramski, D., Gas microbubbles: An assessment of their significance to light scattering in quiescent seas, *Proc. SPIE Int. Soc. Opt. Eng.*, *2258*, 704–710, 1994.

Stramski, D., and D. A. Kiefer, Light scattering by microorganisms in the open ocean, *Prog. Oceanogr.*, *28*, 343–383, 1991.

Stramski, D., R. A. Reynolds, M. Kahru, and B. G. Mitchell, Estimation of particulate organic carbon in the ocean from satellite remote sensing, *Science*, *285*, 239–242, 1999.

Tam, A. C., and C. K. N. Patel, Optical absorption of light and heavy water by laser optoacoustic spectroscopy, *Appl. Opt.*, *18*, 3348–3358, 1979.

Ulloa, O., S. Sathyendranath, and T. Platt, Effect of the particle-size distribution on the backscattering ratio in seawater, *Appl. Opt.*, *33*, 7070–7077, 1994.

Vincent, W. F., R. Rae, I. Laurion, C. Howard-Williams, and J. C. Priscu, Transparency of Antarctic ice-covered lakes to solar UV radiation, *Limnol. Oceanogr.*, *43*, 618–624, 1998.

Zhang, X., M. Lewis, and B. Johnson, Influence of bubbles on scattering of light in the ocean, *Appl. Opt.*, *37*, 6525–6536, 1998.

S. Maritorena, Institute for Computational Earth System Science, University of California, Santa Barbara, CA 93106–3060.

A. Morel, Laboratoire de Physique et Chimie Marines, Université Pierre et Marie Curie, CNRS-INSU, BP 8, 06238 Villefranche-sur-mer, France. (morel@obs-vlfr.fr)